CIPM MRA
Comparison reports

EURAMET.T-S7

Comparison of measurement parameters required in radiance temperature scale realisation from 156 °C to 1100 °C

SUPPLEMENTARY COMPARISON

Any further distribution of this Report must be cited as:
F. Girard *et al* 2026 *CIPM MRA Comparison reports* **03004**

https://doi.org/10.59161/ODCV8968

EURAMET.T-S7 (EURAMET Project No 1457)

Comparison of measurement parameters required in radiance temperature scale realisation from 156 °C to 1100 °C

–

Supplementary Comparison Measurement – **Final Report**

F. Girard [(1)], H. Nasibli [(2)], M. Florio [(1)] and O. Pehlivan [(2)]

[(1)] INRiM – Istituto Nazionale di Ricerca Metrologica, Turin, Italy
[(2)] TUBITAK-UME – Ulusal Metroloji Enstitüsü, Gebze, Türkey

ABSTRACT

This report describes the measurement procedures and results of the EURAMET Project No 1457 – "Comparison of measurement parameters required in radiance temperature scale realisation from 156 °C to 1100 °C".

1. INTRODUCTION

The purpose of this supplementary comparison between INRiM and TUBITAK UME is to undertake an examination of some underlying parameters in temperature scale approximation using an InGaAs-based radiation thermometer over the temperature range from 156 °C to 1100 °C. The parameters to be measured were the size-of-source effect, gain (range) ratios, calibration using fixed-point blackbody sources, and an assessment of the impact on the results of changes in the ambient temperature.
The comparison results will be used to support CMC claims of TUBITAK UME (Turkey) for calibrating 1.6 µm radiation thermometers using fixed-point blackbodies.
The InGaAs-based radiation thermometer, operating at a wavelength of nominally 1.6 µm, was used for the comparison. The thermometer was supplied by INRiM - Istituto Nazionale di Ricerca Metrologica. This was circulated between the participants together with a zinc fixed-point blackbody source, also supplied by INRiM. The latter was used for checking the thermometer before the start and at the end of the measurements at both institutes to confirm the correct performance of the transfer thermometer and to determine any possible drift in the thermometer output.
This report describes the results of the measurements at both laboratory, and compares the results they obtained. Further details of the results, as well as the measurement procedures and the description of the equipment used by each participant, are given in the following.

2. PARTICIPANTS

The NMI participants in the project were:

	Institute	Contact person
1)	INRiM, Italy (Coordinator)	Ferruccio Girard and Michael Florio Tel: +39 011 3919 749 and 373 E-mail: f.girard@inrim.it m.florio@inrim.it
2)	TUBITAK UME, Turkey (Participant)	Humbet Nasibli and Ozlem Pehlivan Yildirim Tel: +90 262 679 5000 and 3412 E-mail: humbet.nasibli@tubitak.gov.tr ozlem.pehlivan@tubitak.gov.tr

3. TRANSFER INSTRUMENTS

The Transfer Standard radiation thermometer TS1, provided by INRiM (Italy), based on an InGaAs two-stage cooled photodiode detector and an additional zinc fixed point blackbody source supplied by INRiM, have been circulated together so that the performance and stability of the transfer standard thermometer has been checked, by each Institute, before and after completing all the requested measurements.
Both instruments, shown in Figures 1 and 2, were self-made by INRiM (formerly IMGC).
Below is a summary of the technical specification and details of the INRiM thermometer and the INRiM zinc fixed-point blackbody source. A complete description of their characteristics can be found in [1, 2, and 3]. Instead, the methodology for the approximation of the ITS-90 temperature scale using the fixed-points technique was first proposed and described in [4].

3.1 INRiM Transfer Standard radiation thermometer TS1

(IMGC Drawing n° 71.00/59 dated 1997/01/23)

Wavelength range:	1.5 μm to 1.7 μm
Temperature range:	150 °C to 1100 °C
Field of view:	5 mm diameter at 470 mm working distance *Note: the working distance should be measured from the target to the front of the objective nose of the radiation thermometer*
Warm-up time:	2 hours from switch-on
Output:	the output is in terms of voltage
Background signal:	measurement should be performed by placing the lens cap on the thermometer nose, taking great care not to touch the front surface of the lens
Dimensions:	170 mm high x 126 mm wide and 400 mm long (including the objective nose)

3.2 INRiM zinc fixed-point blackbody source

(IMGC Drawing n° 70.00/14 dated 1996/10/03)

Blackbody dimensions:	9 mm diameter x 61.5 mm depth with a 120° end cone
Emissivity:	0.99957 (open aperture)
Dimensions:	150 mm x 260 mm x 315 mm
Weight:	5.7 kg, including the Zn ingot

Figure 1: The Transfer Standard thermometer INRiM – TS1.

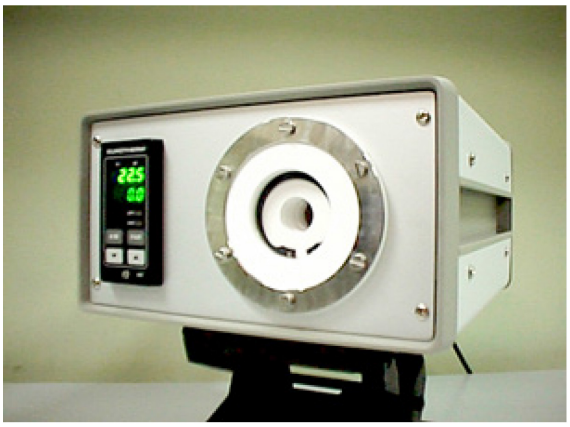

Figure 2: INRiM zinc fixed-point blackbody source.

4. THE SCHEDULE FOR THE CIRCULATION

The original timescale for the circulation of the thermometer was as follows:

Institute	Time periods
INRiM, Italy	1st September 2018 to 31 October 2018
TUBITAK UME, Turkey	1st November 2018 to 31 December 2018
INRiM, Italy	Since 1st January 2019 on

The comparison schedule was delayed, and the circulation periods were modified as follows:

Institute	Updated Time periods
INRiM, Italy	1st September 2018 to 26 November 2018
TUBITAK UME, Turkey	12 December 2018 to 29 September 2020
INRiM, Italy	Since October 15, 2020 on

5. STABILITY CHECK OF THE RADIATION THERMOMETER AT THE ZINC POINT

Prior to the start and at the end of the measurements at both institutes, the transfer thermometer was checked using the INRiM-supplied zinc freezing point blackbody source. The instructions for using the source were supplied and are given in the protocol in Appendix 1. The first melt was used to ensure that the thermometer was aligned correctly on the source; the freeze was used for the stability check measurements. The results of all the checks made by both participants are given in Table 1.

Participant NMI	Date (dd/mm/yyyy)	TS1 Signal @ gain 10^7 V/A (mV)	**Relative temperature difference (°C)**	TS1 Internal temperature (°C)
INRiM (initial)	02/10/2018	1978.403	**0.000**	24.30
	25/10/2018	1977.433	**-0.026**	24.86
	19/11/2018	1976.141	**-0.061**	24.83
UME	22/02/2019	1978.437	**0.001**	20.81
	26/02/2019	1978.459	**0.002**	19.39
	05/03/2019	1978.390	**0.000**	20.63
	18/09/2019	1979.694	**0.035**	26.28
	04/11/2019	1979.143	**0.020**	22.02
	14/05/2020	1976.942	**-0.039**	26.50
UME	09/09/2020	1979.011	**0.016**	23.33
	09/09/2020	1978.872	**0.013**	22.79
UME	10/09/2020	1978.049	**-0.010**	23.37
	10/09/2020	1977.925	**-0.013**	24.24
INRiM (final)	19/10/2020	1976.374	**-0.055**	24.25
	20/10/2020	1976.339	**-0.056**	24.27
	20/10/2020	1976.351	**-0.055**	24.14

Table 1: Results of the zinc point checks for the TS1 thermometer.

The results of the stability check measurements are plotted below (Figure 3). The differences in signal level compared to the start of the comparison (the initial measurements made at INRiM before the thermometer was circulated) were converted to an equivalent temperature, and these values are plotted in Figure 1. They are also given in the fourth column of Table 1. Small fluctuations have been observed, but no significant overall drift. The behaviour of the thermometer signal at the Zn fixed point versus time is similar to those already observed for the same thermometer during preceding comparison exercises [5, 6]. On the INRiM side, corrections have been applied during the calibration process at the fixed-points taking into account for the observed drift at the zinc reference point. Instead, considering the more random distribution of the measured signals during Zn fixed point checks performed at UME, they did not apply any corrections to the signals of the other fixed points. An uncertainty component due to instrument's stability (drift) will be taken into account in the final uncertainty budget. The value of such drift component (u_{19}) reported in Table 15 has been estimated to be 38 mK, and it is derived from the median standard error of all the measurements done using the Zn fixed-point reference at both Institutes during the comparison time.

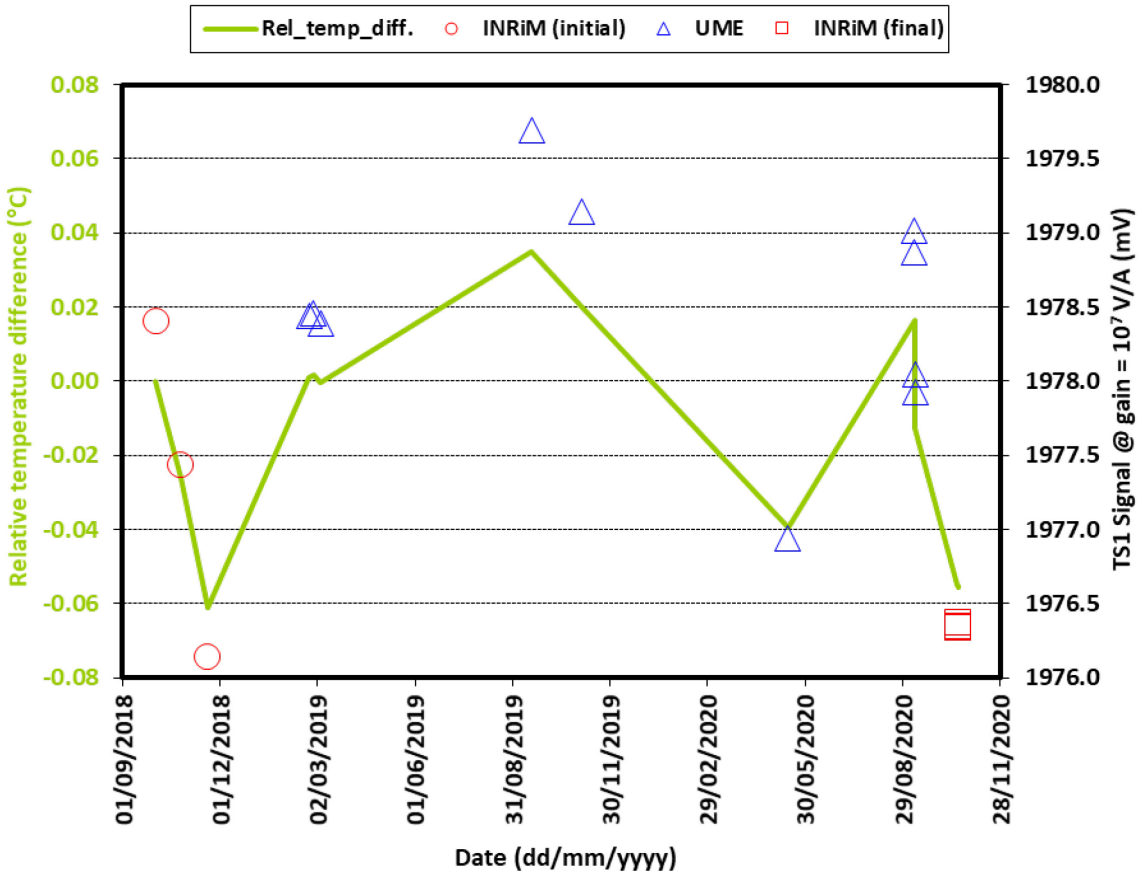

Figure 3: Results of the check measurement at the Zn freezing point for the TS1 thermometer.

6. MEASUREMENT METHODS, RESULTS AND DISCUSSION

6.1 SIZE-OF-SOURCE EFFECT MEASUREMENTS

The size-of-source effect (SSE) measurements were made, at both Institutes, by using the 'indirect' method (with the central portion of the field-of-view of the thermometer obscured by means of a blackened spot or disc). For the SSE measurements, the black spot size used for the TS1 thermometer was 6 mm in diameter. The measurements were performed at 470 mm from the outer surface of the black spot.

The SSE was then calculated using the following equation:

$$SSE(\%) = 100 \cdot \frac{(S_{\text{spot}} - S_{\text{background}})}{(S_{\text{aperture}} - S_{\text{background}})} \quad (1)$$

Where, $S_{\text{background}}$ is the relevant background signal, S_{spot} is the signal measured when the thermometer is aimed at the black spot, and S_{aperture} is the signal when the thermometer is aimed at the sphere, taking into account the transmittance of the window supporting the black spot and the efficiency of the sphere when apertures of different diameters are used. Full details of the apparatus used at each institute are given below.

6.1.1 SSE measurements at INRiM

The size-of-source effect (SSE) was measured using an integrating sphere with a 4" diameter output port as a radiance source. According to the protocol, a set of apertures of different diameters up to a maximum of 100 mm, together with a black spot of 6 mm in diameter, were used. Figures 4 and 5 show a schematic drawing of the device used for the SSE measurements and a picture of the INRiM – TS1 thermometer during the measurement process.

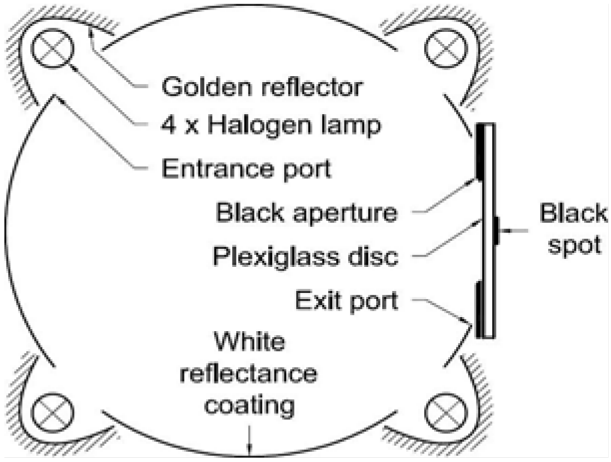

Figure 4: Schematic drawing of the INRiM equipment for measuring the SSE.

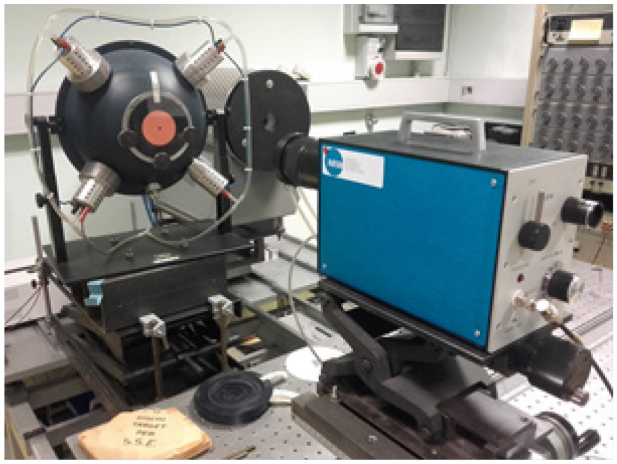

Figure 5: INRiM – TS1 thermometer during the SSE measurement process.

6.1.2 SSE measurements at UME

The SSE measurements were performed on the setup of Figure 6 by employing an integrating sphere (with a diameter of 400 mm) comprising one output port with a diameter of 60 mm. The sphere comprises four incandescent lamps (connected in series) inside. Besides, four internal baffles are placed at specific locations inside the sphere to minimise the specular reflection at the output port of the sphere. The lamps are supplied by a controlled DC current and are switched on at least one hour before the measurements for establishing the quasi-isothermal condition. Apertures with a diameter of 8, 10, 15, 20, 30, 40, 50 and 60 mm were used to imitate a variable–diameter source. A black spot of 6 mm in diameter was used as a target (the obscuration spot).
The black spot is fixed in the middle of a glass window. The transmittance of the spot at the working wavelength band of the thermometer was assessed to be smaller than 0.01 %.

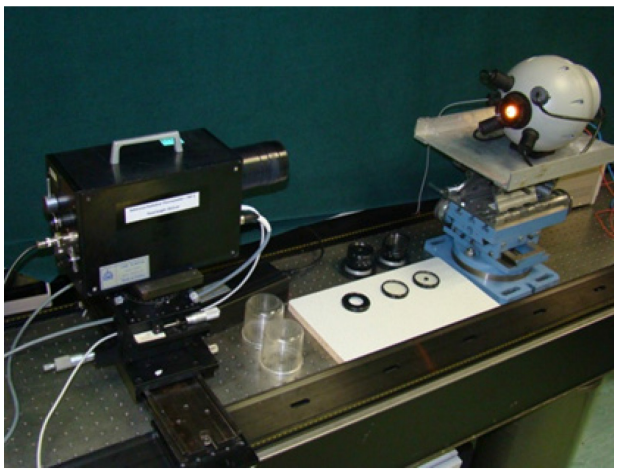

Figure 6: the SSE measurement setup used at UME.

6.1.3 RESULTS OF THE SSE MEASUREMENTS

The results of various SSE measurements made at each institute are summarised in Tables 2 to 4.

Aperture diameter (mm)	INRiM (Feb. 2017) before lens cleaning SSE (%)	$U_{k=2}$ (%)	INRiM (Feb. 2017) after lens cleaning SSE (%)	$U_{k=2}$ (%)
100	0.2197	0.0075	0.1567	0.0053
90	0.2002	0.0068	0.1396	0.0047
80	0.1798	0.0061	0.1218	0.0041
70	0.1592	0.0054	0.1051	0.0036
60	0.1414	0.0048	0.0911	0.0031
50	0.1257	0.0043	0.0803	0.0027
40	0.1096	0.0037	0.0705	0.0024
35	0.1001	0.0034	0.0648	0.0022
30	0.0900	0.0031	0.0590	0.0020
25	0.0791	0.0027	0.0534	0.0018
20	0.0651	0.0022	0.0453	0.0015
15	0.0522	0.0018	0.0390	0.0013
12	0.0415	0.0014	0.0325	0.0011
10	0.0327	0.0011	0.0263	0.0009
8	0.02092	0.00071	0.01693	0.00058

Table 2: Summary of the results of the SSE measurements performed at INRiM, as of February 2017, before and after cleaning the thermometer lens.

Aperture diameter (mm)	INRiM results (Oct. 2018) SSE (%)	$U_{k=2}$ (%)
100	0.1916	0.0065
90	0.1724	0.0059
80	0.1521	0.0052
70	0.1322	0.0045
60	0.1151	0.0039
50	0.1010	0.0034
40	0.0880	0.0030
35	0.0807	0.0027
30	0.0728	0.0025
25	0.0649	0.0022
20	0.0543	0.0018
15	0.0440	0.0015
12	0.0359	0.0012
10	0.0285	0.0010
8	0.0182	0.00062

Table 3: Final results of the SSE measurements performed at INRiM in October 2018.

Aperture diameter (mm)	UME results SSE (%)	$U_{k=2}$ (%)
60	0.1210	0.0032
50	0.1272	0.0034
40	0.1128	0.0030
30	0.0988	0.0026
20	0.0967	0.0026
15	0.0472	0.0013
10	0.0276	0.00073
8	0.0161	0.00043

Table 4: Final results of the SSE measurements performed at UME in September 2020.

Plots of the results of the measurements are given in the following Figure 7, along with the $k = 2$ uncertainty bars.

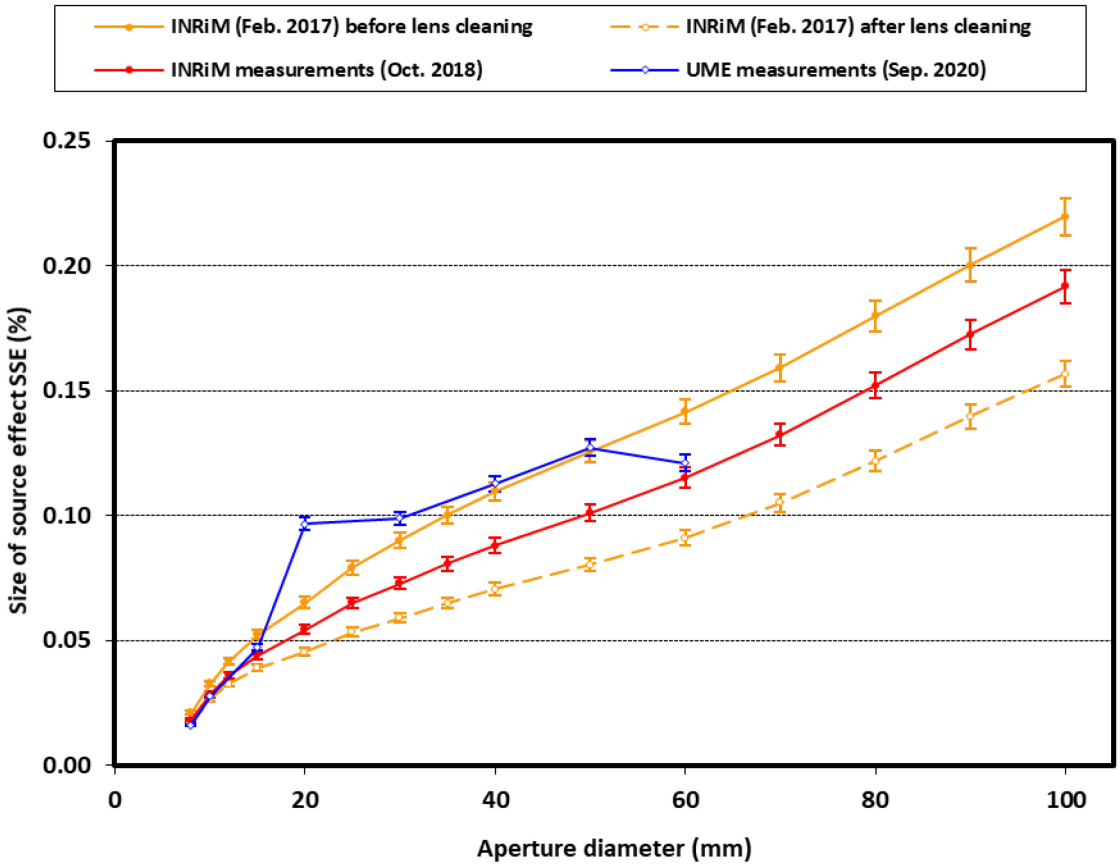

Figure 7: Results of the SSE measurement for the TS1 thermometer.

6.1.4 ANALYSIS OF THE SSE RESULTS, DISCUSSIONS AND CONCLUSIONS

6.1.4.1 Analysis of the results

SSE measurements were made using the size of the apertures available at each institute. INRiM performed SSE measurements in the range of source aperture diameters from 8 mm to 100 mm, while the experimental setup of UME was limited to a maximum source aperture diameter of 60 mm. Considering that the results of the SSE measurements are comparable for both laboratories for the same aperture values, there is no need to make any fittings on the data.
INRiM performed successive SSE measurements over the time (in February 2017 and October 2018) to investigate the effect of dirt that can eventually be deposited on the objective lens of the thermometer. The UME performed only one series of SSE measurements in September 2020, during which three cycles were repeated to estimate the measurement uncertainty (calculated to be $u(\sigma)/\sigma$ = 1.3E-4 by following the approach described in [7]). Other sources of SSE uncertainty taken into consideration by UME were: radiance distribution (valued to be $u(L)/L_0$ = 1E-4), inter-reflection (1.5E-5 was adopted from [8]) and fitting of SSE measured data (7.7E-5 as the root mean square residual of the fourth degree polynomial used for the fitting). The square root of the sum of the uncertainty components cited above gives a result of 1.8E-4 as relative standard uncertainty for the SSE measurement correction. Based on this value, the equivalent temperature corrections were calculated at all fixed points and reported in Table 14.

6.1.4.2 Discussion of the results and conclusions

The orange curves shown on the graph of Figure 7 corresponding to SSE measurements performed before and after the cleaning of the thermometer lens evidenced clearly that the cleaning has an

impact on the SSE measured values and that this impact is larger than the SSE estimated measurement uncertainty.
Apart from the source aperture of 20 mm, where the SSE value measured at UME clearly deviates from the usual trend observed for this type of thermometer [5, 6], the results of the measurements between the two institutes, even if not in full agreement, follow the same trend. The observed differences may be due to an increase over time of dirt on the thermometer lens during the rather long time of the comparison. However, an effect similar to the one observed can also be due to a reflection between the optical components and this could be the evidence of an incorrect SSE experimental measurement setup.
It is recommended to verify that the optomechanical components are aligned in the following order: integrating sphere, aperture, black spot support glass and thermometer. It is easy to verify experimentally that a swap in the order between the glass supporting the black spot and the aperture can give the observed effect, especially for smaller aperture diameters. A confirmation of this effect is the result obtained by UME for the aperture diameter of 60 mm where the integrating sphere was used at full aperture (i.e. without any diaphragm) where the corresponding measured value, lower than expected, clearly deviates from the curve trend. This does not happen in case of INRiM, not even at 100 mm, because a diaphragm limits the full aperture of the sphere (4") while maintaining the same measurement layout.

6.2 GAIN RATIOS MEASUREMENTS

All adjacent gain pairs were measured, starting from 10^{10} V/A down to 10^{4} V/A, even if, during the fixed points calibration of the thermometer, only the range of amplifier gains from 10^{9} V/A to 10^{5} V/A was used.
Specifically, for the fixed-points calibration, the following gain settings were used: 10^{9} V/A at indium and tin fixed points, 10^{7} V/A at zinc fixed point, 10^{6} V/A at the aluminium fixed point and 10^{5} V/A at silver and copper fixed points, respectively.
The value for each gain ratio was then calculated using the following equation:

$$GR\_\mathrm{H/L} = \frac{S(10^{\mathrm{H}}\ \mathrm{V/A}) - S_{\mathrm{background}}(10^{\mathrm{H}}\ \mathrm{V/A})}{S(10^{\mathrm{L}}\ \mathrm{V/A}) - S_{\mathrm{background}}(10^{\mathrm{L}}\ \mathrm{V/A})} \qquad (2)$$

Where, H and L are the respective high and low gain used, and $S_{\mathrm{background}}$ are the relative background signals.
The results of the gain ratios measurements of the thermometer, together with all the additional parameters requested by the protocol, were reported in the template prepared by the coordinator and shown in Tables 5 and 6 for INRiM and UME measurements, respectively.

6.2.1 Apparatus used for the measurements of the gain ratios at INRiM

The INRiM measurements were made using a high stability tungsten ribbon lamp in connection with a suitable combination of neutral density filters mounted on the front of the objective of the thermometer. For each adjacent pair of gains measured, the supply current of the pyrometric High-Stability lamp was regulated such that the output signal of the thermometer was near its full scale (i.e., around to 10 V) on the higher gain (H) and consequently, a corresponding signal of about 1 V was obtained at the lower gain (L). A sequence of ten measurements for each couple of gain ratios was performed in succession at both gains in order to check for measurement repeatability.

Description		**Quantity**	/						
Gain Ratios		Date of meas.	dd/mm/yyyy	21/09/2018	20/09/2018	20/09/2018	19/09/2018	25/09/2018	25/09/2018
	@ Gain	GH / GL	V/A	$10^{10}/10^{9}$	$10^{9}/10^{8}$	$10^{8}/10^{7}$	$10^{7}/10^{6}$	$10^{6}/10^{5}$	$10^{5}/10^{4}$
Average TS1 Output	H	AvgThOut_H	mV	9216.6	9918.99	10207.36	10234.23	10039.9	9860.38
Average TS1 Output StdDev	H	AvgThOut_H_stddev	mV	1.6	0.52	0.94	0.56	1.8	0.22
Average Background	H	AvgBkg_H	mV	1.98	0.045	-0.0701	-0.43145	-0.45448	-0.45515
Average Background StdDev	H	AvgBkg_H_stddev	mV	0.22	0.015	0.0017	0.00031	0.00069	0.00053
Average TS1 Output (corr. for bkg)	H	AvgThOut - AvgBkg	mV	9214.6	9918.95	10207.43	10234.66	10040.3	9860.83
Average TS1 Output (corr. for bkg) StdDev	H		mV	1.7	0.52	0.94	0.56	1.8	0.22
Average TS1 Output	L	AvgThOut_L	mV	999.86	910.827	1014.45	1023.546	1003.77	1005.750
Average TS1 Output StdDev	L	AvgThOut_L_stddev	mV	0.18	0.043	0.11	0.052	0.17	0.078
Average Background	L	AvgBkg_L	mV	0.058	-0.0629	-0.43276	-0.46910	-0.45806	-0.45536
Average Background StdDev	L	AvgBkg_L_stddev	mV	0.017	0.0018	0.00064	0.00073	0.00044	0.00080
Average TS1 Output (corr. for bkg)	L	AvgThOut - AvgBkg	mV	999.80	910.890	1014.88	1024.015	1004.23	1006.206
Average TS1 Output (corr. for bkg) StdDev	L		mV	0.18	0.043	0.11	0.052	0.17	0.078
Gain Ratio Measured Value	**H / L**	**GR_meas_value**		**9.2164**	**10.8893**	**10.0578**	**9.9946**	**9.9981**	**9.8000**
TS1 Internal Temperature		Tint	°C	24.30	24.16	24.23	24.22	24.13	24.21
Ambient Temperature		Tamb	°C	22.8	22.6	22.8	22.6	22.9	22.9
Ambient Relative Humidity		RHamb	%	56	51	51	51	50	49
Gain Ratios (standard relative unc.)		$u_{16}(S_i)/S_i$	%	0.036	0.010	0.020	0.011	0.035	0.010

Table 5: Summary template of INRiM gain ratios measurements.

6.2.2 Apparatus used for the measurements of the gain ratios at UME

Excluding the gain ratio $10^{8}/10^{7}$, for which the measurements were done using the integrating sphere already used in the SSE measurements (switched on at least one hour before the measurements to establish the quasi-isothermal condition and with 10 mm aperture to imitate the fixed-point cavity source), for all other gain ratios the measurements were made using the same set of fixed points available in the lab and used to perform the calibration of the thermometer. By using this approach, the signal corresponding to each fixed point has been measured at the two adjacent gains together with the corresponding background signals. It has to be noted that in this specific case, only with the copper fixed point, the output signal of the TS1 thermometer was near its full scale.

Description		**Quantity**	/						
Gain Ratios		Date of meas.	dd/mm/yyyy	28/09/2020	22/09/2020	29/09/2020	27/09/2020	14/09/2020	29/09/2020
	@ Gain	GH / GL	V/A	$10^{10}/10^{9}$	$10^{9}/10^{8}$	$10^{8}/10^{7}$	$10^{7}/10^{6}$	$10^{6}/10^{5}$	$10^{5}/10^{4}$
Average TS1 Output	H	AvgThOut_H	mV	757.08	1825.214	9107.62	1973.289	5466.831	10844.23
Average TS1 Output StdDev	H	AvgThOut_H_stddev	mV	0.15	0.030	0.20	0.052	0.052	0.04
Average Background	H	AvgBkg_H	mV	-7.48	-1.1639	-0.0527	-0.61955	-0.63016	-0.599
Average Background StdDev	H	AvgBkg_H_stddev	mV	0.12	0.0087	0.0024	0.00059	0.00045	0.051
Average TS1 Output (corr. for bkg)	H	AvgThOut - AvgBkg	mV	764.56	1826.377	9107.673	1973.909	5467.461	10844.83
Average TS1 Output (corr. for bkg) StdDev	H		mV	0.19	0.031	0.20	0.052	0.052	0.06
Average TS1 Output	L	AvgThOut_L	mV	81.919	167.4221	904.903	196.8633	546.1685	1101.4396
Average TS1 Output StdDev	L	AvgThOut_L_stddev	mV	0.016	0.0032	0.020	0.0031	0.0036	0.0042
Average Background	L	AvgBkg_L	mV	-1.030	-0.28453	-0.5935	-0.58800	-0.63168	-0.6377
Average Background StdDev	L	AvgBkg_L_stddev	mV	0.016	0.00059	0.0013	0.00045	0.00042	0.0027
Average TS1 Output (corr. for bkg)	L	AvgThOut - AvgBkg	mV	82.949	167.7066	905.497	197.4513	546.8002	1102.077
Average TS1 Output (corr. for bkg) StdDev	L		mV	0.023	0.0032	0.020	0.0031	0.0037	0.005
Gain Ratio Measured Value	**H / L**	**GR_meas_value**		**9.2173**	**10.89031**	**10.05820**	**9.99694**	**9.99901**	**9.84036**
TS1 Internal Temperature		Tint	°C	21.02	22.51	26.40	23.04	25.65	24.98
Ambient Temperature		Tamb	°C	20.3	21.3	22.2	22.0	24.2	22.4
Ambient Relative Humidity		RHamb	%	46	61	45	43	44	45
Gain Ratios (standard relative unc.)		$u_{16}(S_i)/S_i$	%	0.053	0.0036	0.0045	0.0042	0.0016	0.0010

Table 6: summary template of UME gain ratios measurements

The results of gain ratios measurements made at each institute are summarized in Table 7 where the normalised error is also reported in the last column (E_n). The results are shown in graphical form in Figure 8, along with the k = 2 uncertainty bars.

Gain ratio	INRiM value	INRiM $U_{k=2}$	UME value	UME $U_{k=2}$	E_n
$10^{10}/10^{9}$	9.2164	0.0066	9.2173	0.010	0.074
$10^{9}/10^{8}$	10.8893	0.0022	10.89031	0.00079	0.44
$10^{8}/10^{7}$	10.0578	0.0040	10.05820	0.00090	0.10
$10^{7}/10^{6}$	9.9946	0.0021	9.99694	0.00084	1.0
$10^{6}/10^{5}$	9.9981	0.0069	9.99901	0.00032	0.14
$10^{5}/10^{4}$	9.8000	0.0020	9.84036	0.00020	20

Table 7: Summary of the gain ratio values, expanded uncertainties and normalized error.

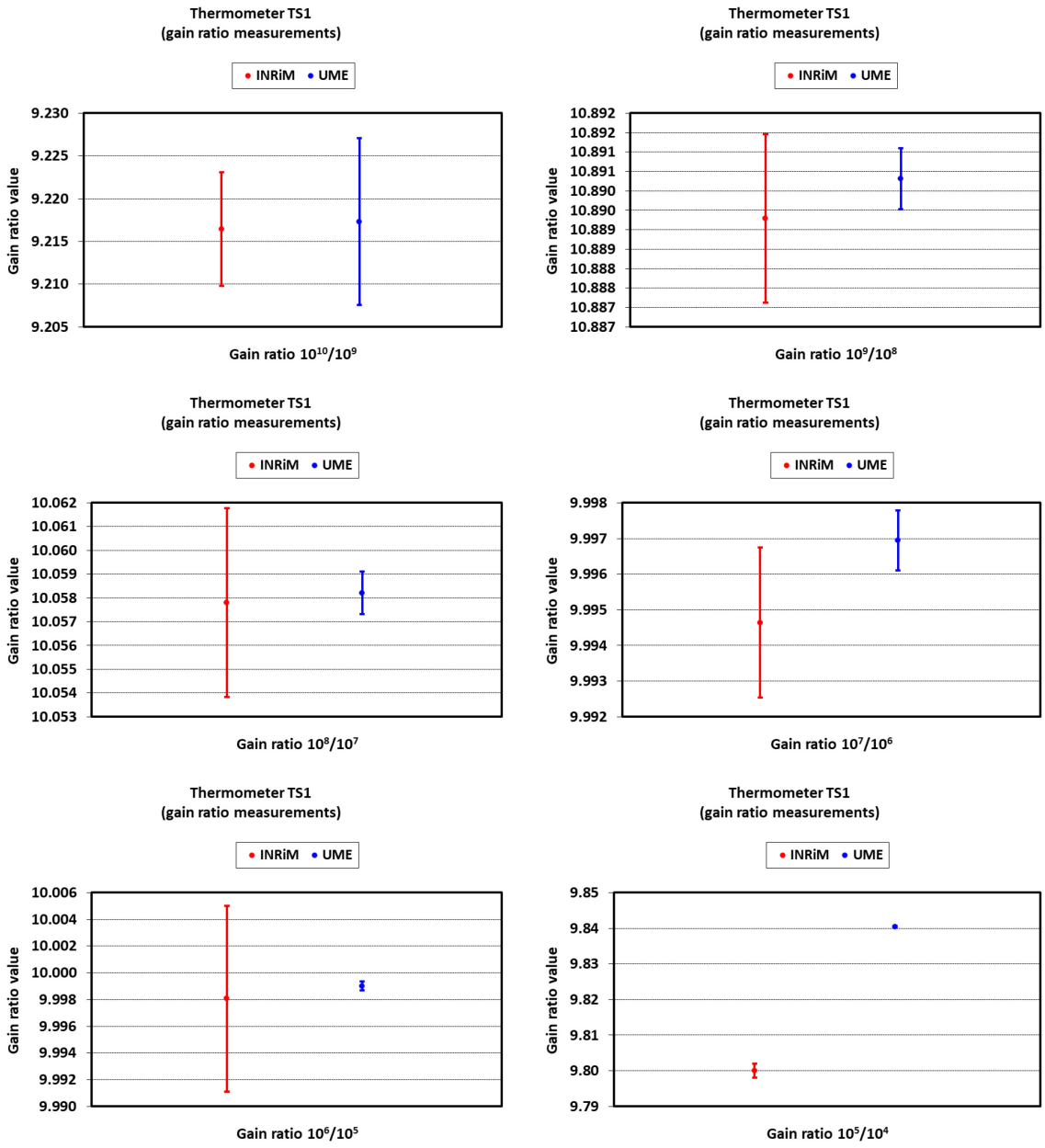

Figure 8: Results of the gain ratios measurement for the TS1 thermometer.

6.2.3 Discussion of the results

The different sources of radiation adopted by the two institutes, namely: high stability tungsten ribbon lamp for INRiM and fixed points for UME, in carrying out the measurements of the gain ratios

are the basis of the different declared measurement uncertainties. Despite this, the majority of the measurement results are in reasonably good agreement. Practically for all gains used in this comparison exercise, ranging from 10^9 V/A down to 10^5 V/A, the value of the normalised error is below the unit. An outlying data point has been observed for the measurements of the gain ratio 10^5 V/A onto 10^4 V/A, for which the cause is unknown.

6.3 EFFECT OF AMBIENT CONDITIONS

The results of the measurements of the ambient temperature effect on the thermometer, together with all the additional parameters requested by the protocol, were reported in the template prepared by the coordinator and shown in Tables 8 and 9 for INRiM and UME measurements, respectively.

6.3.1 Effect of ambient temperature – INRiM measurements

The measurement of the effect of changes in ambient temperature on the output of the thermometer was performed simply by changing the room temperature of the entire laboratory.
As a set point for the air condition system of the laboratory, three different nominal temperatures were used: 18 °C, 23 °C and 28 °C respectively. Moreover, to ensure a good thermal homogeneity of both the thermometer and measuring instruments, a waiting time of 24 hours has been introduced between the change in temperature of the lab and the start of each measurement cycle. Following the protocol, INRiM started measurements with the fixed point of zinc as a reference source. The effect of ambient temperature on the output signal of the thermometer was measured by repeating, on successive days, three melt/freeze plateaux of the fixed points of tin, zinc, silver and copper for each of the ambient temperature values reported above. Because the thermometer is very little affected by ambient condition changes, to reduce the measurement uncertainty, only the results corresponding to the lower and higher room temperature values settings (i.e. 18 °C and 28 °C) were finally used to calculate the effects due to the change of ambient temperature. Considering the very limited effect, especially at lower source temperatures, INRiM did not apply any correction for source temperatures below the fixed point of the tin.

Description	**Quantity**	*I*												
Effect of Ambient Conditions	Date of meas.	dd/mm/yyyy	04/10/2018	03/10/2018	05/10/2018	04/10/2018	02/10/2018	05/10/2018	10/10/2018	08/10/2018	11/10/2018	12/11/2018	07/11/2018	14/11/2018
Source nominal temperature	Source nom. temp.	°C	232 (Sn fixed point)			420 (Zn fixed point)			960 (Ag fixed point)			1084 (Cu fixed point)		
Average TS1 Output	AvgThOut	mV	1827.979	1830.487	1836.649	1979.534	1978.150	1977.073	5644.38	5641.40	5632.47	10858.18	10849.40	10835.649
Average TS1 Output StdDev	AvgThOut_stddev	mV	0.079	0.088	0.071	0.056	0.043	0.079	0.40	0.61	0.15	0.22	0.58	0.018
Average Background	AvgBkg	mV	-2.4133	0.097	5.684	-0.4187	-0.41968	-0.4275	-0.4517	-0.4872	-0.5249	-0.45457	-0.48509	-0.53670
Average Background StdDev	AvgBkg_stddev	mV	0.0081	0.054	0.032	0.0018	0.00015	0.0016	0.0013	0.0018	0.0022	0.00080	0.00080	0.00080
Average TS1 Output (corr. for bkg)	AvgThOut - AvgBkg	mV	1830.392	1830.39	1830.97	1979.953	1978.570	1977.501	5644.84	5641.89	5632.99	10858.63	10849.89	10836.185
Average TS1 Output (corr. for bkg) StdDev		mV	0.087	0.14	0.10	0.058	0.043	0.081	0.40	0.61	0.15	0.22	0.58	0.019
Ambient Nominal Temperature	Amb. Nom. Temp.	°C	18 (Low)	23 (Mid)	28 (High)	18 (Low)	23 (Mid)	28 (High)	18 (Low)	23 (Mid)	28 (High)	18 (Low)	23 (Mid)	28 (High)
TS1 Internal Temperature	Tint	°C	19.91	24.27	30.11	19.81	24.30	30.08	24.57	27.84	33.12	25.10	28.51	33.66
TS1 Internal Temperature StdDev	Tint_stddev	°C	0.17	0.15	0.15	0.13	0.06	0.04	0.10	0.01	0.04	0.01	0.01	0.12
Ambient Temperature	Tamb	°C	17.6	22.8	28.6	17.6		28.6	18.7		26.7	17.8	22.7	26.7
Ambient Relative Humidity	RHamb	%	59	40	35	59		35	61		40	66	50	30
TS1 Output Change	ΔThOut	mV		0.57			-2.45			-11.84			-22.45	
TS1 Output Change StdDev	ΔThOut_stddev	mV		0.19			0.14			0.55			0.24	
TS1 Internal Temperature Change	ΔTint	°C		10.20			10.27			8.55			8.56	
TS1 Internal Temperature Change StdDev	ΔTint_stddev	°C		0.32			0.17			0.14			0.13	
Ambient Temperature Effect	ΔThOut / ΔTint	mV/°C		**0.056**			**-0.239**			**-1.385**			**-2.623**	
Amb. Temp. Effect (standard relative unc.)	$u_{14}(S_i)/S_i$			0.363			0.073			0.064			0.026	

Table 8: Summary template of the effect of ambient temperature – INRiM measurements.

6.3.2 Effect of ambient temperature – UME measurements

At UME, the zinc-point signals were acquired from the plateau realisations by placing the TS1 thermometer inside a climatic chamber (Weiss WKL1000/70/5-LN2) and the fixed-point furnace outside the chamber (there is a hole of a diameter of about 10 cm on the side wall of the chamber). The set point temperature of the climatic chamber was set so that the internal temperature of the TS1 thermometer reaches and stabilises at the temperatures of 18 °C, 23 °C and 28 °C, respectively.

Effect of Ambient Conditions	Date of meas.	dd/mm/yyyy	27/09/2020	27/09/2020	27/09/2020
Source nominal temperature	Source nom. temp.	°C	420 (Zn fixed point)		
Average TS1 Output	AvgThOut	mV	1976.784	1973.289	1971.338
Average TS1 Output StdDev	AvgThOut_stddev	mV	0.010	0.052	0.010
Average Background	AvgBkg	mV	-0.5548	-0.61955	-0.61056
Average Background StdDev	AvgBkg_stddev	mV	0.0015	0.00059	0.00092
Average TS1 Output (corr. for bkg)	AvgThOut - AvgBkg	mV	1977.339	1973.909	1971.948
Average TS1 Output (corr. for bkg) StdDev		mV	0.011	0.052	0.011
Ambient Nominal Temperature	Amb. Nom. Temp.	°C	18 (Low)	23 (Mid)	28 (High)
TS1 Internal Temperature	Tint	°C	18.05	23.08	28.06
TS1 Internal Temperature StdDev	Tint_stddev	°C	0.01	0.11	0.07
Ambient Temperature	Tamb	°C	16.8	22.2	27.5
Ambient Relative Humidity	RHamb	%	59	49	41
TS1 Output Change	ΔThOut	mV		-5.39	
TS1 Output Change StdDev	ΔThOut_stddev	mV		0.02	
TS1 Internal Temperature Change	ΔTint	°C		10.01	
TS1 Internal Temperature Change StdDev	ΔTint_stddev	°C		0.08	
Ambient Temperature Effect	ΔThOut / ΔTint	mV/°C		**-0.539**	
Amb. Temp. Effect (standard relative unc.)	$u_{14}(S_i)/S_i$			0.012	

Table 9: Summary template of the effect of ambient temperature – UME measurements.

The effect of the ambient temperature on the signal output of the thermometer at the other fixed points has been obtained by calculations based on the Zn fixed-point measurements results using the following UME procedure:
By using the measured data at the Zinc point at three different ambient temperatures, summarised in the following table,

Tint (°C)	S (mV)
18.05	1977.339
23.08	1973.909
28.06	1971.948

The magnitude of the ambient temperature effect on the output signal at the Zn fixed point has been obtained:

$$\frac{\Delta S}{\Delta t} = -0.54 \text{ mV/°C} \tag{3}$$

Then, by dividing this ratio by the signal at the Zinc fixed-point and the ambient temperature at 23°C, a corresponding output signal change per 1 °C change of the ambient temperature may be obtained:

dS(mV)/dt Zn	-5.4E-01
dS/Sdt Zn	-2.7E-04

$$\frac{\Delta S}{S\Delta t} = -0.00027 \text{ °C}^{-1} \tag{4}$$

Finally, the signals obtained at other fixed-points can be corrected by multiplying this coefficient $\Delta S/(S\Delta t)$ by the fixed-point signal.
Afterwards, two different methods to convert temperature differences can be applied:

First method: using the Wien approximation of the Planck law by using $\Delta S/S$ in place of $\Delta L/L$ and obtaining the corresponding temperature differences:

$$\Delta T = \frac{\lambda T^2}{c_2} \cdot \frac{\Delta S}{S} \tag{5}$$

Second method: using the Sakuma-Hattori equation to obtain the temperature corrections:

$$\Delta T = \left(\frac{c_2}{A \cdot \ln\left((C/S)+1\right)} - \frac{B}{A} \right) - \left(\frac{c_2}{A \cdot \ln\left((C/(S-\Delta S))+1\right)} - \frac{B}{A} \right) \tag{6}$$

The two methods give negligible differences in the calculated temperature corrections. The results obtained are reported in the following Table 10.

FPs	t (°C)	T (K)	Tint (°C)	Gain	S_meas (mV)
In	156.5985	429.7485	22.37	1.0976E+09	82.9685
Sn	231.928	505.078	22.81	1.0976E+09	1825.69
Zn	419.527	692.677	22.54	9.9435E+06	1977.06
Al	660.323	933.473	25.01	1.0065E+06	5464.48
Ag	961.78	1234.93	24.79	1.0004E+05	5641.62
Cu	1084.62	1357.77	25.63	1.0004E+05	10860.7

Note: this table was split only to improve the page layout

FPs	S_meas / Gain (V)	dS/dt (mV/°C)	(S/dt)*(25 °C - Tint)	dT(K) Radiance (per 1°C)	dT(K) Sakuma (per 1°C)	dT(K) Sakuma (25 °C - Tint)
In	7.5594E-11	-2.2637E-02	-5.9535E-02	-0.006	-0.006	-0.015
Sn	1.6634E-09	-4.9812E-01	-1.0906E+00	-0.008	-0.008	-0.017
Zn	1.9883E-07	-5.3942E-01	-1.3290E+00	-0.015	-0.015	-0.036
Al	5.4291E-06	-1.4909E+00	1.2508E-02	-0.027	-0.027	0.000
Ag	5.6393E-05	-1.5392E+00	-3.2075E-01	-0.047	-0.047	-0.010
Cu	1.0856E-04	-2.9632E+00	1.8665E+00	-0.056	-0.057	0.036

Table 10: Calculated effect of the ambient temperature at all fixed points, based on measurements made at the Zinc fixed-point at UME.

6.3.3 ANALYSIS OF THE RESULTS, DISCUSSION AND CONCLUSIONS

The measurement results of the effect of ambient temperature, performed in both institutes, are numerically summarised in Table 11 and graphically represented in Figure 9, together with the respective expanded uncertainty bars.

FPs	t_{90} (°C)	TS1 radiance sensitivity		INRIM measurements			UME measurements		
		(%/°C)	(mV/°C)	ΔS/ΔTint (mV/°C)	ΔT/ΔTint (°C/°C)	$U_{k=2}$ (°C/°C)	ΔS/ΔTint (mV/°C)	ΔT/ΔTint (°C/°C)	$U_{k=2}$ (°C/°C)
In	156.5985	4.869	4.1	-/-	-/-	-/-	-0.023	-0.006	0.00019
Sn	231.928	3.525	64.5	0.056	0.0009	0.00063	-0.498	-0.008	0.00026
Zn	419.527	1.874	37.1	-0.239	-0.0064	0.00094	-0.539	-0.015	0.00035
Al	660.323	1.032	56.5	-1.148(*)	-0.020(*)	-/-	-1.491	-0.026	0.00090
Ag	961.78	0.590	33.2	-1.385	-0.042	0.0053	-1.539	-0.046	0.0016
Cu	1084.62	0.488	52.9	-2.623	-0.050	0.0026	-2.963	-0.056	0.0019

Table 11: Results of the effect of ambient temperature.

(*) *Note: values based on a 2nd order polynomial fit of the measurements made at the fixed points of Sn, Zn, Ag and Cu and used to apply the corrections for* Tref = 25 °C *at Al shown in Table 12.*

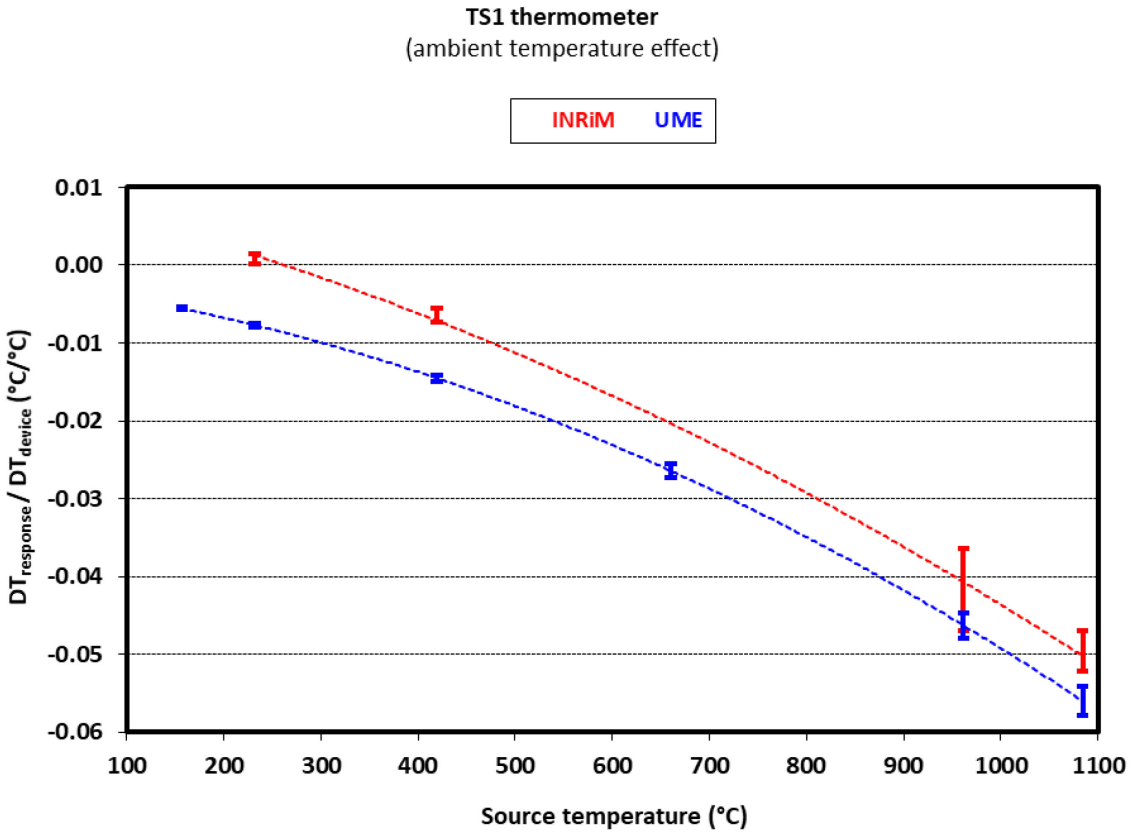

Figure 9: TS1 thermometer – results of the effect of ambient temperature.

Analysing the curves shown in Figure 9, there is clear evidence that the measured trend of the effect of the ambient temperature on the thermometer signal for different source temperatures, is similar in the behaviour, even if the measured value(s) are not completely consistent with each other. Only at the fixed point of silver there is an agreement of the values within the combined uncertainty between the measurements performed in both institutes. This is mainly due to quite different estimated uncertainties, some of which are derived from experimental data in the case of INRiM and others calculated based on experimental measurements performed only at the fixed point of zinc, in the case of UME. For both institutes, the measured and/or calculated values of the ambient temperature effect were then used, during the thermometer calibration process, to correct for the internal temperature at all fixed points to refer the measured signals to the same internal temperature of the instrument (i.e. 25 °C), as the protocol requires it.

6.4 FIXED-POINT CALIBRATION

The TS1 thermometer has been calibrated at INRiM and UME following the laboratory's usual local procedure using the fixed-points blackbody sources of: In, Sn, Zn, Al, Ag and Cu. A sequence of three complete melt/freeze cycles has been performed for each fixed-point.
For each fixed-point, a scan across the blackbody aperture has been performed with the thermometer during a melt and freeze plateau to assess the surrounding temperature profiles. These profiles were then used to perform the appropriate corrections based on the size-of-source effect measurements. The correction was calculated using the laboratory's usual method, starting from the actual fixed-point blackbody aperture diameter up to the reference target diameter specified by the protocol (i.e. 20 mm).

6.4.1 Description of the INRiM equipment used

6.4.1.1 Fixed-point cells

Six different fixed-point blackbody cells, namely: In, Sn, Zn, Al, Ag and Cu, were used. All the cells were of the same design, described in [3] and [4], with an available inner volume of about 48 cm^3. The blackbody cavities used have a cylindrical shape of 9 mm in diameter and a length of 61.7 mm terminated with an additional cone of 120° included angle. The effective normal emissivity of the cavity was calculated assuming the value of 0.88 (with an estimated standard uncertainty of 0.02) for the emissivity of the graphite walls, and a value of 0.99957 was found (with an associated relative standard uncertainty of 0.00010). The indium, tin and zinc cells were filled with 6N pure metals; instead, for aluminium, silver and copper cells, 5N metals were used.

6.4.1.2 Fixed point furnaces

Two different types of furnaces were used for the fixed-point calibrations. A set of three compact fixed-point furnaces specifically designed for realising scales at low-temperatures was used for the indium, tin and zinc points [3]. All these furnaces were of the same type as the one used to check the stability of the thermometer at the fixed zinc point during the comparison. A schematic diagram of the furnace interior is shown in Figure 10, where it is possible to see how the crucible is contained in an aluminium shell, which acts as a temperature-equalising block. In this way, the temperature distribution along the crucible proved to be uniform within about 1 °C.

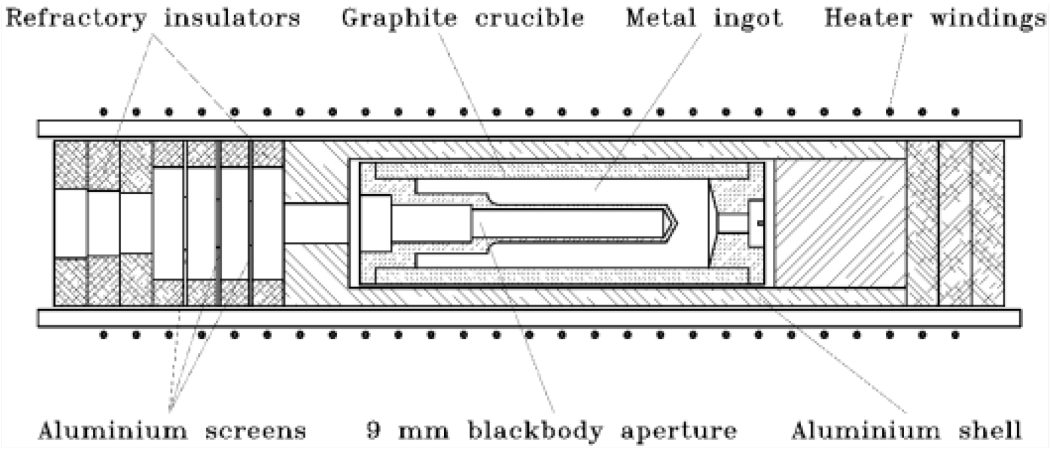

Figure 10: Interior scheme of INRiM In, Sn and Zn fixed point blackbody furnace.

A three-zone heating furnace, Carbolite model TZF 12/65/550, was employed to realise the aluminium, silver and copper points. Quartz tubes, one for each fixed point, were used to accommodate the rear insulating parts, the crucibles and the front sacrificial graphite rings. Properly adjusting the furnace control parameters for each independent heating zone allows temperature uniformity better than 1 °C to be obtained over the entire crucible length.

6.4.2 Fixed points calibration – INRiM results

As recommended by the protocol, the following measurement procedure was adopted: for each fixed point, three successive melt/freeze cycles have been performed, and the respective output signals, background signals and internal temperature of the thermometer have been recorded and averaged.
These signals were then corrected, in the order, for:

a) the calculated effective emissivity of the cavity (0.99957 ± 0.00010);

b) the drift versus time observed at the zinc fixed-point reference temperature. The corrections have been done by taking as a normalization point the last Zn fixed point realised on November 19, 2018 and assuming a constant relative output change in terms of radiance at the other fixed points.

For this purpose, Figure 11 shows a graphical representation of the stability of the thermometer signal at the zinc fixed-point temperature as a function of time during all the periods of measurements performed at INRiM. A nearly linear drift of the thermometer output signal, corresponding to about 0.06 °C, has been observed. In the same figure are also reported:

- the thermometer's drift after that the correction for ambient temperature effect has been applied (note: TS1 internal reference temperature Tref. = 25 °C);
- the coefficients of the linear fittings used to apply the relative correction for drift to the corresponding measured output signals at the other fixed points during the calibration (note: the coefficients are based and expressed in terms of Excel's absolute time);
- the corresponding dates, marked by the green symbols, on which the thermometer calibration was performed at the other fixed points.

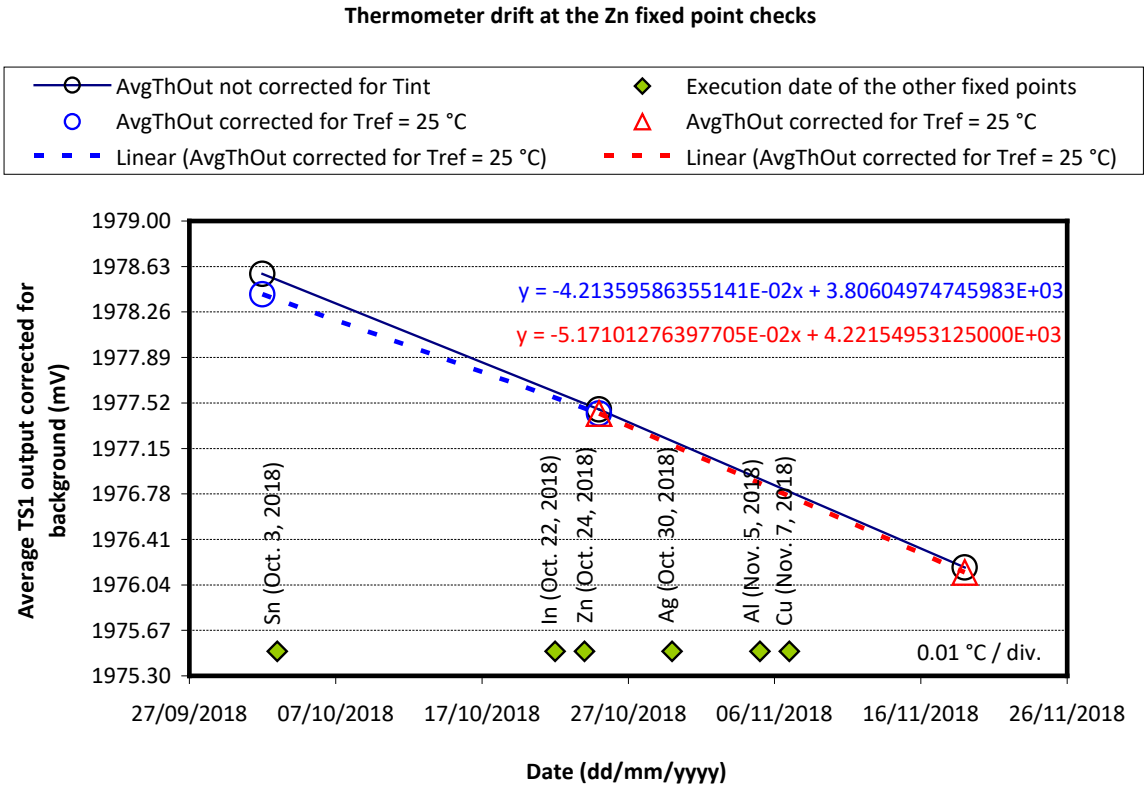

Figure 11: Drift at the zinc fixed point of the TS1 thermometer during the measurements performed in the INRiM labs.

c) the difference between the internal temperature of the thermometer and the reference internal temperature (the correction has been applied based on the results of the measurements of the ambient temperature effect).

Moreover, at all fixed points, an automatic scan across the furnace aperture has been executed with the thermometer during an additional melt/freeze plateau to access the surrounding temperature profiles (note that a circular symmetry has been assumed and only a scan from left to right has been executed). The results, both, in terms of radiance and temperature distribution, are reported in Figures 12 and 13, respectively.

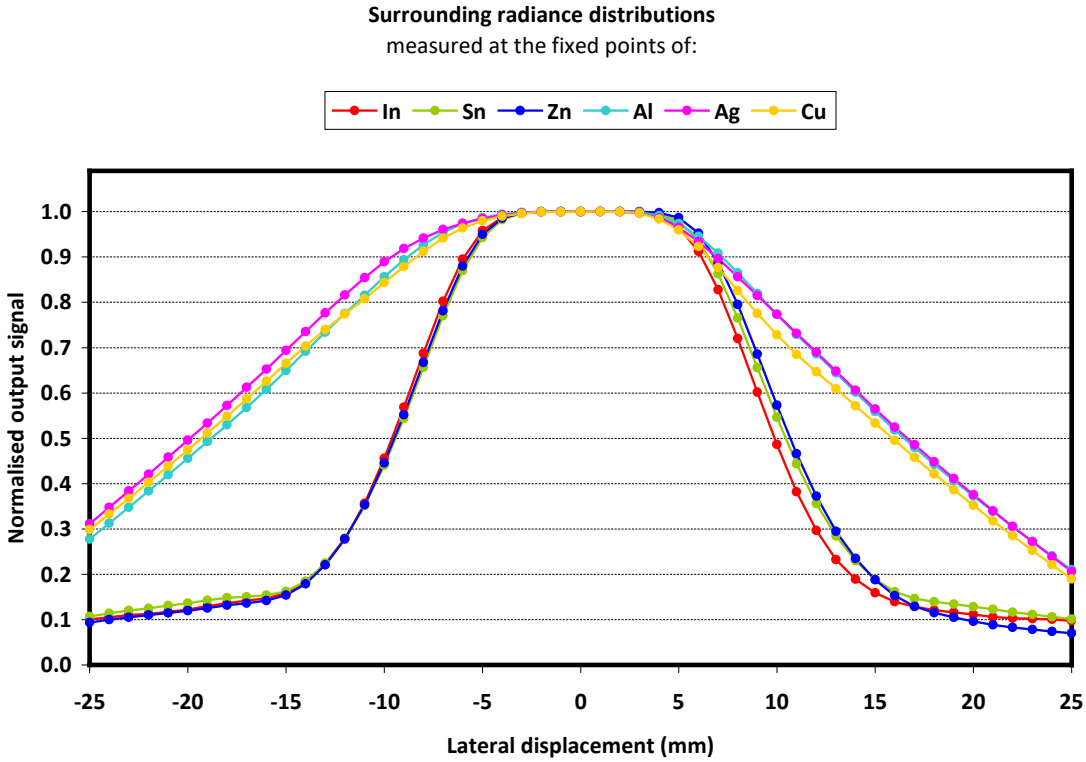

Figure 12: INRiM measurements of the lateral radiance distribution of the fixed-point sources.

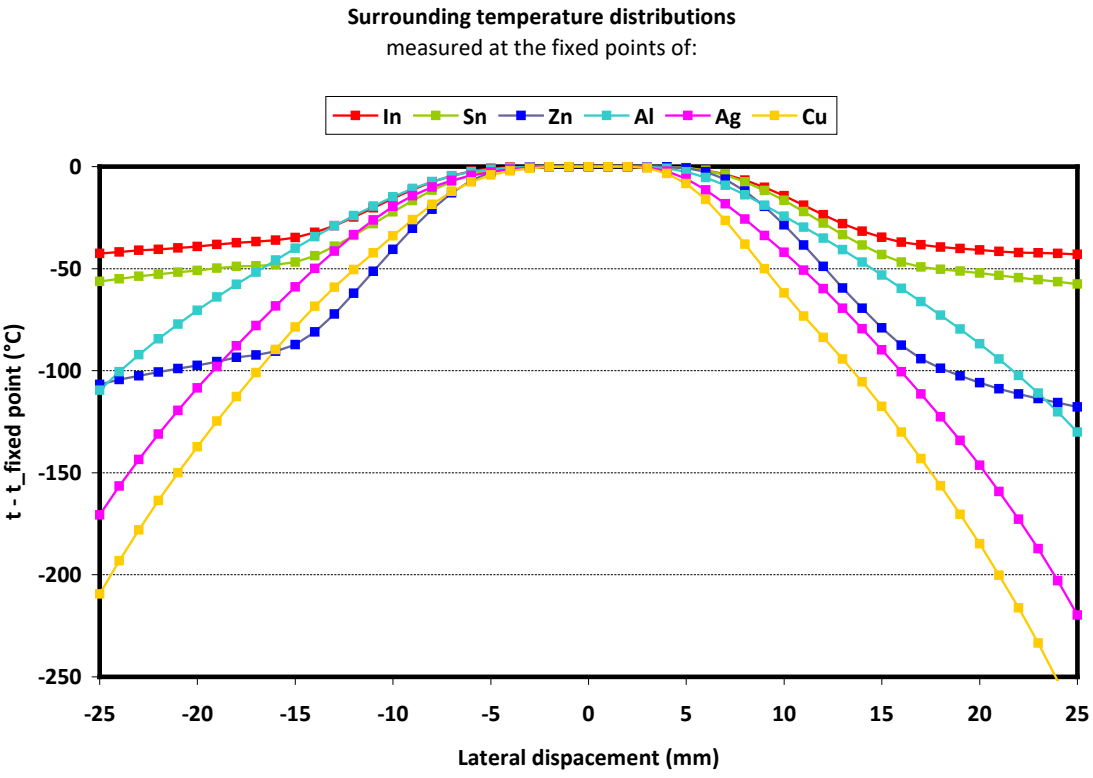

Figure 13: INRiM measurements of the temperature distribution of the fixed-point sources.

From Figure 12 is easy to discern two families of curves corresponding to the two different kinds of furnaces used for the calibration at the fixed points of: In, Sn, Zn and for Al, Ag and Cu, respectively. Based on lateral radiance/temperature distributions measured, a further correction for:

d) size-of-source effect will be then calculated and applied to thermometer output signals at each fixed point by using the procedure described below.

As recommended by the protocol, the output signal of the thermometer has to be normalised, for each fixed point, to a reference source with a nominal aperture diameter of 20 mm.

The calculation of the SSE correction to be applied was done based on the following steps:

- the radiance distribution has been considered constant inside the aperture of the blackbody cavity so that no correction was applied for source diameters less than 9 mm;
- the measured SSE data were first fitted using a fourth-degree polynomial to derive the intermediate SSE values corresponding to the lateral displacement positions
- for source diameters ranging from 9 mm up to 20 mm a positive SSE correction factor was calculated based on the size-of-source effect measured for each ring (with a thickness of 1 mm measured on the radius), divided by the measured radiance distribution (normalised) in the same corresponding area of the source;
- for source diameters ranging from 20 mm up to 50 mm a negative SSE correction factor was calculated based on the size-of-source effect measured for each ring (with a thickness of 1 mm measured on the radius), multiplied by the measured radiance distribution (normalised) in the same corresponding area of the source;
- contributions from radiance sources diameters larger than 50 mm were not considered.

For each fixed point, the SSE correction in terms of thermometer output signal was reported in Table 12.

The calibration results at the fixed points were collected together with all the parameters and corrections to the thermometer output signals, and the template was consequently filled in. It is summarised in the following Table 12.

	Quantity	/						
		xls abs time	43395	43376	43397	43409	43403	43411
Fixed Points Calibration	Date of meas.	dd/mm/yyyy	22/10/2018	03/10/2018	24/10/2018	05/11/2018	30/10/2018	07/11/2018
INRiM	Fixed Point		In	Sn	Zn	Al	Ag	Cu
	FP temperature	°C	156.5985	231.928	419.527	660.323	961.78	1084.62
	TS1 Sensitivity	%/°C	4.8691338	3.5250359	1.8742129	1.0319934	0.5896520	0.4877845
	Gain used 10^X	V/A	9	9	7	6	5	5
Description								
Average TS1 Output	AvgThOut	mV	83.707	1830.487	1977.271	5472.658	5637.66	10849.40
Average TS1 Output StdDev	AvgThOut_stddev	mV	0.028	0.088	0.073	0.045	0.13	0.59
Average Background	AvgBkg	mV	0.218	0.097	-0.41979	-0.45752	-0.48107	-0.48509
Average Background StdDev	AvgBkg_stddev	mV	0.013	0.054	0.00078	0.00071	0.00056	0.00080
Average TS1 Output (corrected for bkg)	AvgThOut - AvgBkg	mV	83.489	1830.39	1977.691	5473.116	5638.14	10849.89
Average TS1 Output (corrected for bkg) StdDev		mV	0.031	0.10	0.073	0.045	0.13	0.59
TS1 Internal Temperature	Tint	°C	24.35	24.27	24.63	25.17	27.24	28.51
Ambient Temperature	Tamb	°C	22.9	22.8	22.9	22.9	22.9	22.7
Ambient Relative Humidity	RHamb	%	36	40	42	54	38	50
Fixed Point Cavity Emissivity	ε_cav		0.99957	0.99957	0.99957	0.99957	0.99957	0.99957
TS1 output correction for ε cavity	corr_ε_cav	mV	0.036	0.79	0.850	2.353	2.42	4.67
		°C	0.009	0.012	0.023	0.042	0.073	0.088
TS1 output correction for Zn drift	corr_Zn_drift	mV	-0.060	-2.06	-1.336	-2.005	-2.95	-3.41
		°C	-0.015	-0.032	-0.036	-0.035	-0.089	-0.064
TS1 output correction for Tref = 25 °C	corr_Tref_25°C	mV	0.000	0.04	-0.088	0.195	3.10	9.21
		°C	0.000	0.001	-0.002	0.003	0.093	0.174
TS1 output correction for SSE to Ø Ap. = 20 mm	corr_SSE_Ø=20	mV	0.027	0.57	0.603	0.583	0.56	1.29
		°C	0.007	0.009	0.016	0.010	0.017	0.024
TS1 output corrected for the parameters above	**TS1_out**	**mV**	**83.492**	**1829.73**	**1977.720**	**5474.243**	**5641.28**	**10861.64**

Table 12: Fixed points calibration – INRiM final results

6.4.3 Description of the UME equipment used

6.4.3.1 Fixed point cells

Six different metal fixed-point blackbodies, having identical geometrical configurations and construction, were used in the comparison. The cells were filled with high-purity metals, namely In, Sn, Zn, Al, Ag and Cu. The fixed-point blackbodies and crucibles were made from high-purity graphite with less than 10 ppm ash content and a density higher than 1.8 g/cm^3. The blackbodies have a cylindrical cavity with an aperture of 9 mm in diameter and 61.5 mm in height. The back wall of the cavities has a cone shape with a 120° included angle. The emissivity of the cavities was estimated as about 0.9998 by assuming a value of 0.95 for the emissivity of graphite and isothermality during phase transitions.

6.4.3.2 Fixed point furnaces

Two different furnaces, one very similar to that described in [3], and the other a three-zone open-ended alumina tube furnace, were used to perform the fixed point realisations. The first furnace is used to realise the In, Sn and Zn fixed points. In this furnace, the crucible container is an aluminium cylinder, which acts as a temperature-equalising block and allows a temperature uniformity of 1 °C along the crucible [3]. Besides, the geometry of the aperture and the use of low-emissivity material, such as aluminium, in the immediate surroundings of the blackbody aperture minimises the contribution of stray radiation

The second furnace, with an internal diameter of 65 mm and heating length of 600 mm, utilising indirect heating by wire resistance heating elements, was used to realise the Al, Ag and Cu fixed points. Glass wool and two graphite blocks (approximately 1.5 cm thick) were placed behind the cell to reduce the effect of heat transfer from the cell location to the outside. Two similar blocks with cylindrical viewing holes slightly larger than the aperture of the cavity were placed in front of the cell. Several bored-out ceramic rings with internal diameters larger than the field-of-view of the thermometer (to avoid vignetting of the radiation thermometer) were placed on the front. Finally, a specially designed T-shaped cap made from bored-out ceramic—with an internal diameter that exceeds the thermometer's field of view and an external head diameter larger than the furnace tube diameter—is used to shield the pyrometer from stray light, particularly that transmitted via quartz tube walls acting as waveguides at high temperatures, as shown in Figure 14 a).

The furnace, which can operate up to 1200 °C under these atmospheric conditions (with argon gas), has three heaters in the middle zone and two heaters in each end zone. Prior to fixed-point realisation, a series of experiments were done to determine optimum furnace offsets to minimise the temperature gradients along the length of the furnace tube. The temperature profile along the heating tube was measured by using a dummy cell, which was made from a high-density graphite cylindrical block, and has a length, and external and internal diameters of 200 mm, 50 mm, and 3 mm, respectively. The block was placed inside the furnaces instead of a crucible in the configurations described in Figure 14 a). Figure 14(b) illustrates an image of the Cu fixed-point cell and the crucible used for this point (left three items). A similar configuration was employed for the Ag and Al fixed points. The only difference is that the crucible cap of the Al point has a hole with a diameter of approximately 11 mm, whereas for the Ag and Cu points the hole diameter is approximately 15 mm. The inner bore of the block serves as the borehole for a type S thermocouple (without sealed housing) mounted on a motorised linear displacement stage and used to measure the furnace temperature profile. By adjusting the offsets of the side zones, the temperature uniformity in this middle zone (with a length of about 20 cm) better than 1 °C was obtained.

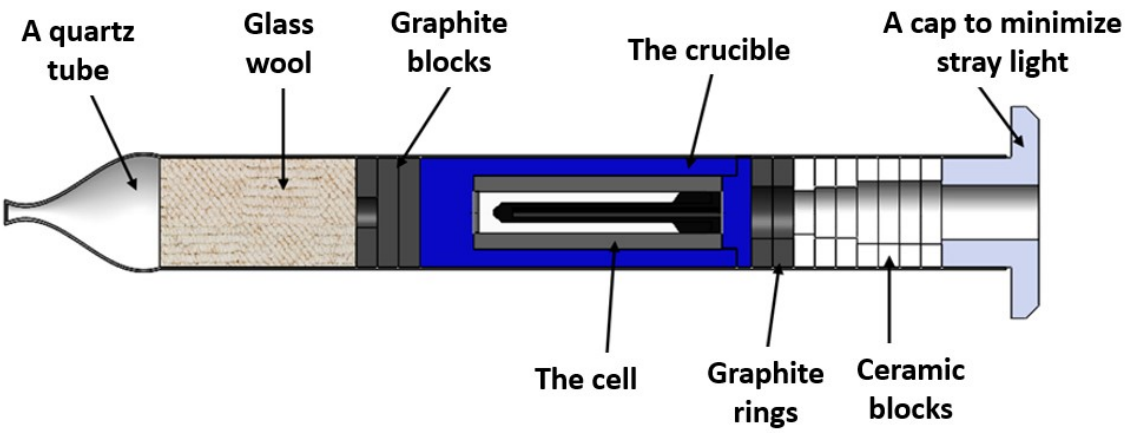

(a)

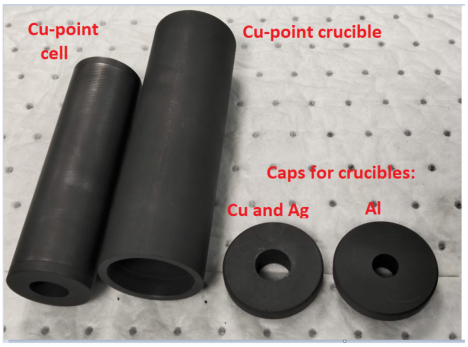

b)

Figure 14: a) Schematic illustration of the crucible (of Al, Ag and Cu Fixed points) inside the heating tube of the three-zone furnace; b) Image of Cu point cell, the crucible and its cap.

6.4.4 Fixed points calibration – UME results

UME performed the fixed-point calibrations in September 2020 and, according to the protocol, realised three successive runs of melt and freeze for each fixed point. The respective output signals, background signals and internal temperature of the thermometer have been collected, averaged and reported in the spreadsheet prepared by the coordinator, together with all other information required.

The net measured signals were corrected for the effective emissivity of the cavity, estimated to be 0.9998. UME did not apply any correction for the thermometer signal drift from the zinc fixed-point reference temperature during the thermometer calibration. A correction for ambient temperature effect was applied at all fixed points taking into account the difference between the internal temperature of the thermometer and the internal reference temperature (i.e. 25 °C). The corrections applied for the effect of the ambient temperature have been calculated for all other temperatures of the fixed points on the basis of the measurements made experimentally only at the zinc fixed point. To make the signal corrections due to the SSE, a horizontal and vertical scans of the furnace surface was performed at each fixed point using an automatic motorised translation stage with a travel of 10 cm. This allows performing the measurements of the (radiance)

temperature across the furnace aperture in both directions up to where the signal diminishes to near zero level.

The results of these scans (normalised to max signal, i.e. to the signal corresponding to the respective fixed point) are shown in Figures 15 to 18. Please note that for the Cu and Ag fixed points, the plateau region is wider than that of the Al fixed point. This is due to the larger hole diameter in the crucible caps of Cu and Ag fixed points, as shown in Figure 14 b).

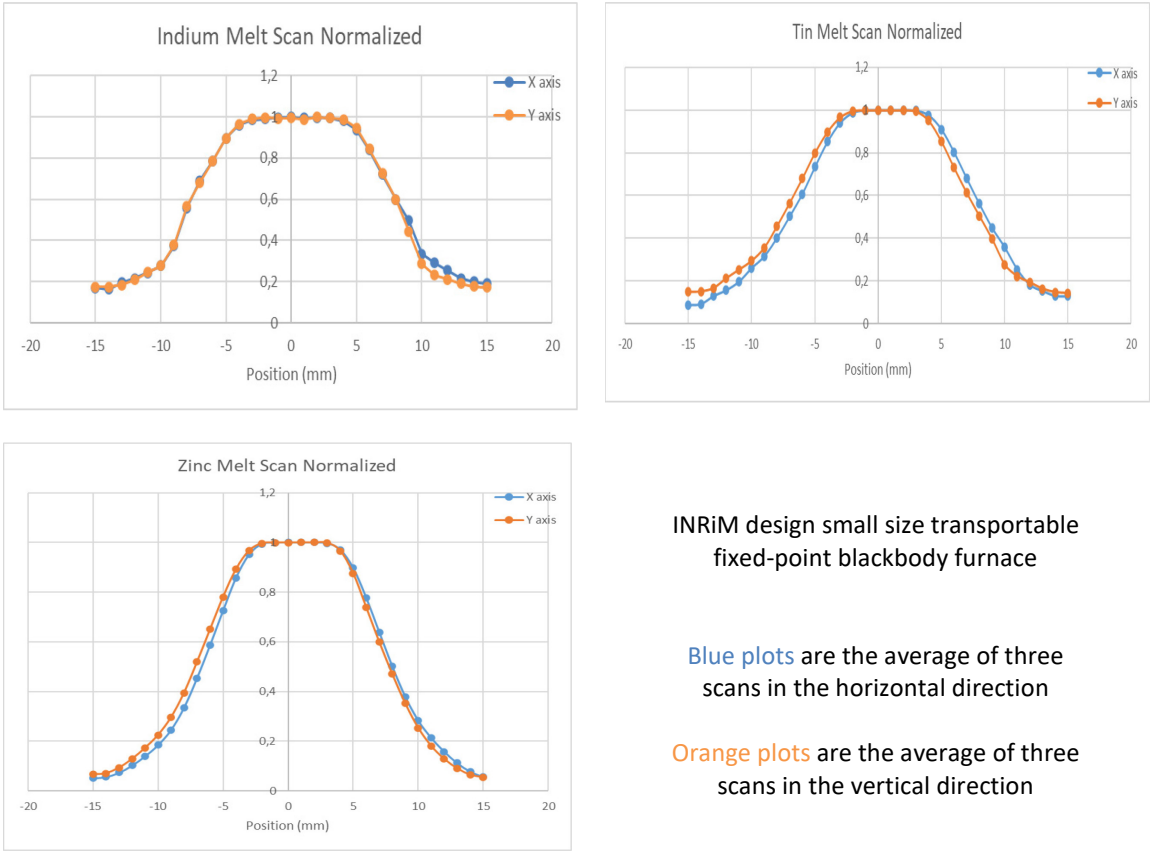

Figure 15: Normalised average of three scans of the thermometer's output signal across the cavity at the horizontal (the blue curves) and vertical (the orange curves) directions at the melting temperature of the In, Sn, and Zn fixed-points (Furnace type 1).

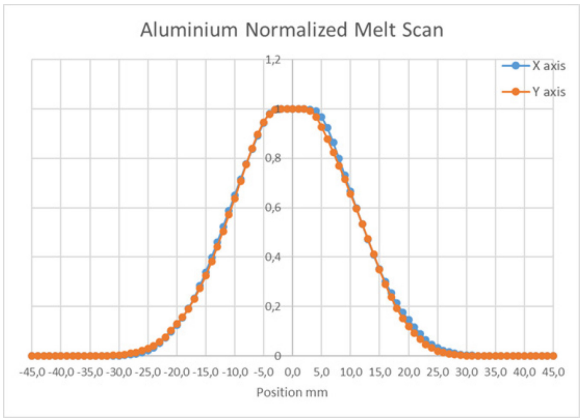

Figure 16: Normalised average scans across the cavity (at the horizontal and vertical directions) at the melting temperature of Al fixed-point (Furnace type 2).

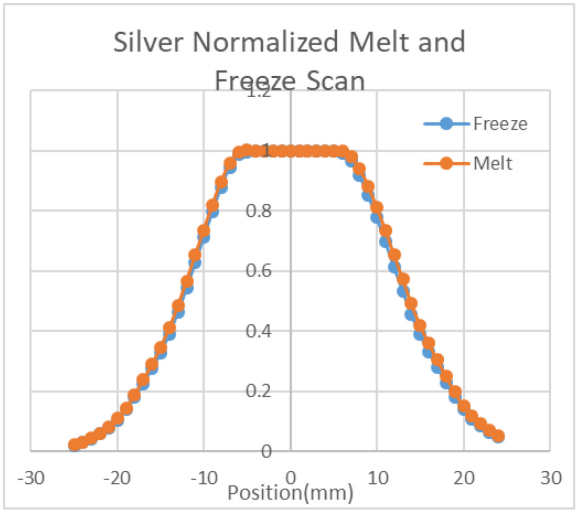

Carbolite three-zone furnace
Ag fixed-point inside a quartz tube

Blue plots are the average of two freeze scans in the horizontal direction

Orange plots are the average of two melt scans in the horizontal direction

Figure 17: Normalized average scans across the cavity (at the horizontal and vertical directions) at the melting temperature of Ag fixed-point (Furnace type 2).

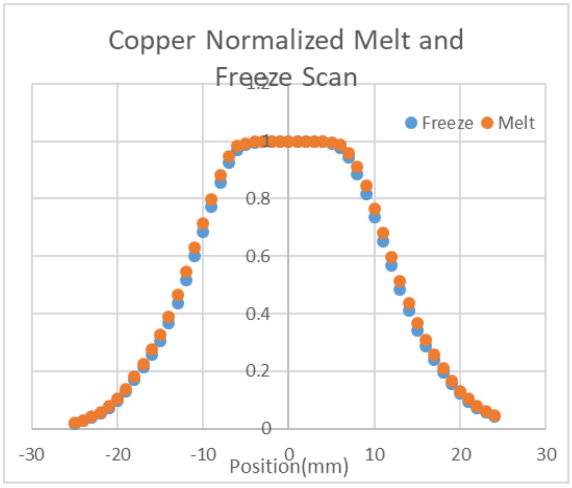

Carbolite three-zone furnace
Cu fixed-point inside a quartz tube

Blue plots are the average of three freeze scans in the horizontal direction

Orange plots are the average of three melt scans in the horizontal direction

Figure 18: Normalised average scans across the cavity (at the horizontal and vertical directions) at the melting temperature of Cu fixed-point (Furnace type 2).

As recommended by the protocol, the output signal of the thermometer has to be normalised, for each fixed point, to a reference source with a nominal aperture diameter of 20 mm. The calculation of the SSE correction was performed according to the following steps:

1. The radiance distribution is considered constant within the 9 mm blackbody aperture, and no correction is applied for source diameters below this threshold.
2. Contribution of the radiance from outside of the blackbody aperture diameter to the nominal aperture diameter (green area) should be added to the measured signal.
3. Contribution of the radiance from outside of the nominal aperture diameter to a larger diameter (red area) should be subtracted from the reference corrected signal.
4. Translate the RT in a way that the viewing spot of the RT is located just outside of the cavity, as it is shown in Figure 19. The translation length equal to 6 mm;
5. measure the signal at this point and add the SSE correction in terms of signal for an annular ring with an inner diameter of 9 mm and outer diameter of 20 mm (green area), which is shown as a grey circle in Figure 19. We assume that the signal detected by the RT corresponds to the

average radiance within the grey spot as temperature decrease is linear in this area, and this radiance has a radial symmetry around the cavity;

6. Calculation Formula: The correction coefficients are determined by applying the difference formula $SSE(d_2, d_1) = SSE(d_2, d_0) - SSE(d_1, d_0)$, where $d_0 = 6$ mm is the diameter of the RT viewing spot, $d_1 = 9$ mm and $d_2 = 20$ mm, a first correction coefficient can be calculated;
7. then now, the reference and target diameter are equal. By repeating the 5th and 6th steps for the next annular ring (red area) but this time subtracting the result, the final correction coefficient can be calculated.

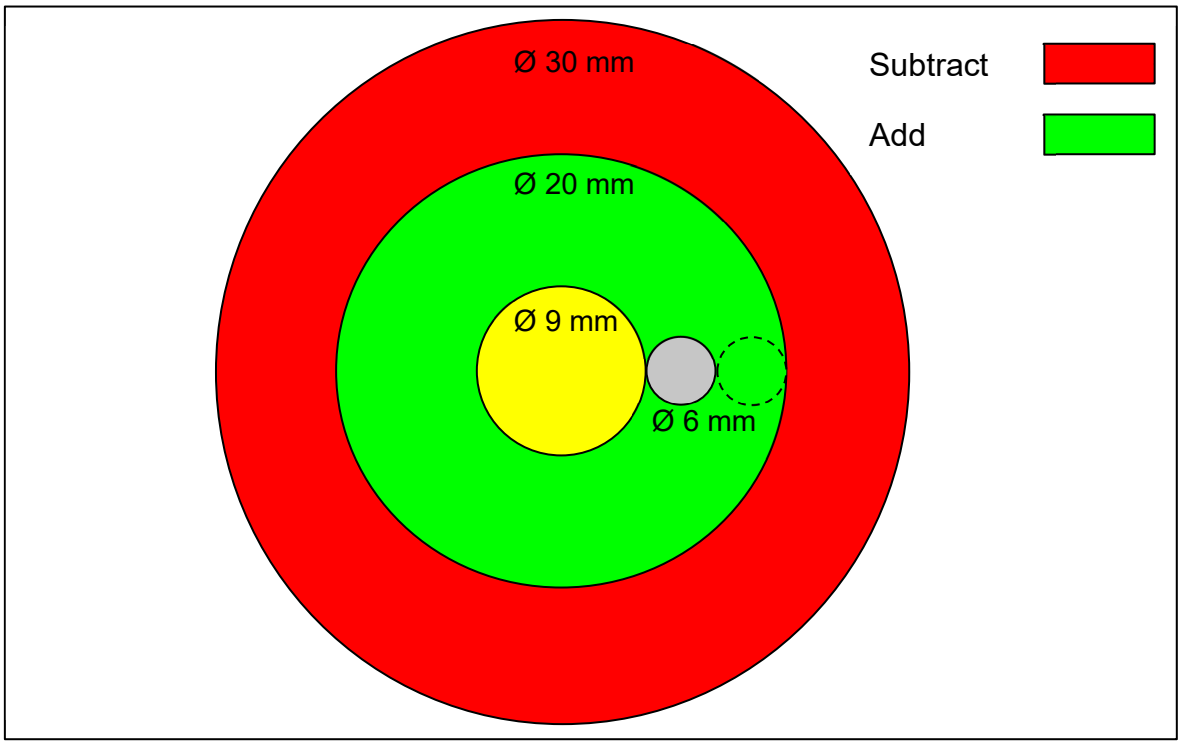

Figure 19: SSE correction scheme.

By using averaged melt scan signals of In, Sn, Zn, Al, Ag and Cu and the procedure cited above, it is possible to determine the SSE correction to be applied to the thermometer output signals measured at the fixed-points in order to refer each one at a source reference diameter of 20 mm as requested. The uncorrected thermometer signals and the respective corrected signals, signal differences and corresponding temperature differences are reported in Table 13.

Fixed-point	T (K)	Gain 10^x (V/A)	TS1 raw signal (V)	TS1 corrected signal (*) (V)	Signal difference (*) (mV)	Temperature difference (*) (mK)
Indium	429.7485	9	0.082926	0.082939	0.014	3.4
Tin	505.078	9	1.82497	1.82539	0.43	6.7
Zinc	692.677	7	1.97613	1.97660	0.46	12.6
Aluminium	933.473	6	5.46559	5.46536	-0.23	-4.1
Silver	1234.93	5	5.64243	5.64202	-0.41	-12.3
Copper	1357.77	5	10.8647	10.8642	-0.50	-9.4

(*) up to a reference source diameter of 20 mm

Table 13: SSE correction for TS1 thermometer, according to protocol, for a reference target diameter of 20 mm.

The results of the calibration at the fixed points were collected together with all the parameters and corrections to the thermometer output signals and reported in Table 14.

	Quantity	/						
		xls abs time	44093	44096	44085	44087	44088	44100
Fixed Points Calibration	Date of meas.	dd/mm/yyyy	19/09/2020	22/09/2020	11/09/2020	13/09/2020	14/09/2020	26/09/2020
UME	Fixed Point		In	Sn	Zn	Al	Ag	Cu
	FP temperature	°C	156.5985	231.928	419.527	660.323	961.78	1084.62
	TS1 Sensitivity	%/°C	4.8691338	3.5250359	1.8742129	1.0319934	0.5896520	0.4877845
	Gain used 10^X	V/A	9	9	7	6	5	5
Description								
Average TS1 Output	AvgThOut	mV	82.023	1825.01	1976.467	5463.86	5640.9	10860.0
Average TS1 Output StdDev	AvgThOut_stddev	mV	0.016	0.36	0.004	0.20	1.4	2.2
Average Background	AvgBkg	mV	-0.945	-0.68	-0.59530	-0.6282	-0.6973	-0.6259
Average Background StdDev	AvgBkg_stddev	mV	0.016	0.01	0.00059	0.0019	0.0095	0.0029
Average TS1 Output (corrected for bkg)	AvgThOut - AvgBkg	mV	82.968	1825.69	1977.062	5464.48	5641.6	10860.7
Average TS1 Output (corrected for bkg) StdDev		mV	0.022	0.36	0.004	0.20	1.4	2.2
TS1 Internal Temperature	Tint	°C	22.37	22.81	22.54	25.01	24.79	25.63
Ambient Temperature	Tamb	°C	21.16	21.58	20.93	23.36	21.82	21.98
Ambient Relative Humidity	RHamb	%	52.65	50.89	51.22	52.69	57.64	46.30
Fixed Point Cavity Emissivity	ε_cav		0.9998	0.9998	0.9998	0.9998	0.9998	0.9998
TS1 output correction for ε cavity	corr_ε_cav	mV	0.017	0.37	0.395	1.093	1.13	2.17
		°C	0.004	0.006	0.011	0.019	0.034	0.041
TS1 output correction for Zn drift	corr_Zn_drift	mV	0.000	0.00	0.000	0.000	0.00	0.00
		°C	0.000	0.000	0.000	0.000	0.000	0.000
TS1 output correction for Tref = 25 °C	corr_Tref_25°C	mV	-0.060	-1.09	-1.327	0.013	-0.32	1.87
		°C	-0.015	-0.017	-0.036	0.000	-0.010	0.035
TS1 output correction for SSE to Ø Ap. = 20 mm	corr_SSE_Ø=20	mV	0.014	0.43	0.464	-0.231	-0.41	-0.50
		°C	0.003	0.007	0.013	-0.004	-0.012	-0.009
TS1 output corrected for the parameters above	**TS1_out**	**mV**	**82.939**	**1825.39**	**1976.595**	**5465.36**	**5642.02**	**10864.21**

Table 14: Fixed points calibration – UME final results.

7. ESTIMATED MEASUREMENT UNCERTAINTIES

The uncertainty components are expressed following the outline and recommendations provided in the document of CCT-NCTh (formerly CCT-WG5) on Radiation Thermometry – "Uncertainty budgets for the calibration of radiation thermometers below the silver point" [9]. The same uncertainty components numbering used in the already mentioned document [9] was maintained for clarity of exposition.

Table 15 summarises all the uncertainty components that need to be considered for the calibration of a radiation thermometer using the fixed-point blackbody scheme and contains some additional details on how each uncertainty component was evaluated/estimated by each Institute.

u_i	**INRiM**	**UME**
Impurities $u_2(T_i)$	Considering that only indium, tin and zinc cells were filled with 6N pure metals and moreover, that chemical analysis has not been made after the filling, in order to be precautionary, temperature uncertainty values have been considered those recommended as "normal" in [9] for 5N pure metals for all the cells.	At UME, all cells (which were involved in the current comparison) were filled with 5N pure metals, except the Zn fixed point blackbody, which has 6N purity metal. No chemical analysis has been made before and after the filling. Again, except for the Al point, all cells are in intensive usage for more than 20 years. Therefore in the calculations of the total uncertainty for all fixed points, the uncertainty components due to impurity were taken two times more than recommended as "normal" values in [9].

u_i	**INRiM**	**UME**
Plateau identification $u_3(T_i)$	Temperature uncertainty values ranging from 2 mK to 10 mK are recommended for "best" and "normal" realisations, respectively. The values, for the INRiM – TS1 thermometer, are between these limits. Such values have been calculated taking into account the standard deviation associated with the net output signals for the three successive plateaux realised during the calibration process for each fixed point.	The uncertainty component originating from plateau identifications was calculated as the standard deviation associated with the corrected output signals for the three successive plateaux realised during the calibration process for each fixed point. The fixed-point temperature was estimated as the average between 25 % and 75 % solid fraction of the freeze plateau. The results of the first melt-freeze cycle were not included in the data analysis.
Blackbody emissivity, isothermal $u_4(T_i)$	The uncertainty due to the blackbody emissivity arises from the corresponding uncertainty in the surface emissivity value of the graphite constituting the cavity walls. Knowing the geometrical shape of the fixed-point cavity and assuming that the blackbody cavity be isothermal, a consequently relative uncertainty on the calculation of the integrated emissivity of the cavity will derive. The corresponding temperature uncertainty is then obtained based on the sensitivity of the thermometer at the different temperatures for each fixed point, respectively.	The effective emissivity of the cavities was calculated using blackbody emissivity modelling software (from Virial Inc.) based on the Monte Carlo ray-tracing method (STEEP3 is employed for the conic-ended cavities). In the calculations, the emissivity of the graphite in the spectral range from 1.5 µm to 1.7 µm is taken to be ε = 0.9. The uncertainty value of the calculated effective emissivity was evaluated by considering the uncertainty contributions by the graphite and surface emissivity values, geometrical imperfections, dimensional errors of the cavities, and the temperature gradients along the cavity. The corresponding temperature uncertainty is then obtained based on the sensitivity of the thermometer at 1.6 µm at the different temperatures for each fixed point, respectively.
Reflected ambient radiation $u_6(T_i)$	Considering the relatively high effective emissivity of the fixed points blackbody cavity and the wavelength at which the thermometer operates (nominally 1.6 µm), the effect of reflected ambient radiation may be considered negligible at all source temperatures higher than that of indium. For the calibration at the indium fixed-point temperature, an additional uncertainty contribution of 2 mK was considered for any possible ambient reflection effect, even if the optical path between the furnace and the thermometer was screened during the calibration process.	The measurements were performed in a dedicated laboratory room with no windows at all. During the measurements at In, Sn and Zn fixed points, the room illumination was switched off. Taking into account the only ambient radiation at the effective room temperature of about 23 °C, the relatively high effective emissivity of the fixed points blackbody cavity and the working wavelength of the thermometer at nominally 1.6 µm, the correction due to the reflection error in terms of temperature and the associated uncertainty in applying this correction were considered negligible at all source temperatures including the In fixed point.

u_i	**INRiM**	**UME**
Cavity bottom heat exchange $u_7(T_i)$	The temperature drop caused by the radiant heat exchange and conductive heat flow has been calculated as stated in [9] using the equation: $$\Delta T_b = \varepsilon_{tot}\,\sigma\left(T_i^4 - T_a^4\right)\,\frac{d}{\kappa}\,\left(\frac{r}{L}\right)^2$$ where ΔT_b is the temperature drop, ε_{tot} is the total emissivity of the cavity wall, σ is the Stefan-Boltzmann constant, T_i is the blackbody temperature, T_a is the ambient temperature, d is the thickness of the cavity bottom, κ is thermal conductivity of the cavity material, r is aperture radius and L is the cavity length. Considering that the largest contribution to the uncertainty in this correction comes from the assumed value for the thermal conductivity of the graphite and from the uncertainty in the thickness of the cavity bottom, as precautionary criteria, the calculated value for this correction was assumed as uncertainty at the different fixed point's temperatures.	The radiant energy exchange through the cavity aperture produces a temperature drop at the cavity bottom, depending on the blackbody temperature with respect to the ambient temperature. While the aperture of the cavities can be considered relatively larger (about 9 mm), the temperature drop ΔT caused by the radiant heat exchange and the associated uncertainty component should be considered. The crucible of all used cells has a relatively long cavity length, was made from a high-quality graphite material and was machined with considerable accuracy. Therefore, for the corresponding uncertainty components, the 'best' values recommended in [9] were used in the evaluations.
Size-of-source-effect correction $u_{11}(T_i)$	Referring to the apparatus used for the SSE measurement at INRiM, the following uncertainty components that have been taken into account for the determination of the final size-of-source effect measurement uncertainty budget: - Radiance uniformity of the source 1.5 % - Radiance stability of the source 0.05 % - Non-blackness of the black spot 0.2 % - Dimension of the black spots 0.01 % - Dimension of the aperture diaphragms 0.04 % - Aiming and orientation 0.6 % - Signals measurement, repeatability 0.5 % Total combined standard uncertainty 1.7 % **Total extend uncertainty U_{sse} (k = 2) 3.4 %**	UME, based on its SSE measurement apparatus, has estimated the following uncertainty components: - SSE measurement uncertainty $1.3\cdot10^{-4}$ [7] - Radiance distribution $u(L)/L_0 = 1 \cdot 10^{-4}$ - Inter-reflections $1.5 \cdot 10^{-5}$ [8] - SSE fitting $7.7 \cdot 10^{-5}$ From these uncertainty components the total combined relative uncertainty for SSE corrections is calculated as $\frac{u_{11}(S_i)}{S_i} = 1.84\cdot10^{-4}$, which results in $(u_{11}(T_i))$ 3.8 mK, 5.2 mK, 9.8 mK, 18 mK, 31 mK and 38 mK for the In, Sn, Zn, Al, Ag and Cu fixed point measurements, respectively. *Note: uncertainties related to mechanical dimensions of the apertures and obscuration, concentricity and residual transmission of the black spot are not considered because their contribution is negligibly small.*

u_i	**INRiM**	**UME**
Non-linearity $u_{12}(T_i)$	The non-linearity measurement was not in the aims of the present comparison. Moreover, preceding works have shown that InGaAs detectors are linear if used with underfilling of the diode's sensitive area [10, 11]. A detailed description of the investigation of the linearity on the output signal of this thermometer may be found in [11]. However, in order to take into consideration also this possible effect, the standard deviation of the repeatability of non-linearity measurement of $5 \cdot 10^{-5}$ was taken as a relative uncertainty value. Using this value and the calculated sensitivities of the thermometer at each fixed point, the corresponding values of uncertainty in temperature have been derived.	The non-linearity measurement of two different InGaAs-based radiation thermometers, both having a very similar configuration and the same type of photodetector as the transfer standard artefact, were studied thoroughly in [12]. The results of this work, as well as those of [12], have shown that the InGaAs detectors demonstrate significant non-linearity over the whole working range in overfilled illumination conditions. However, the measurements in the underfilled illumination condition (with an aperture of the diameter of 1.9 mm in front of the detector) didn't reveal any non-linearity behaviour within the measurement uncertainty of less than 10^{-5}. Taking into account the optical design of the radiation thermometer with a field stop in the front of the detector (that prevents the detector from the overfilled illumination condition), the radiation thermometer can be regarded as linear. According to these results, no non-linearity corrections were applied to the FP calibration outputs of the thermometer.
Ambient temperature correction $u_{14}(T_i)$	The final uncertainty budget for this component was derived by propagating the relative standard deviations of the differences in the measured internal temperatures of the thermometer and the relative standard deviations of the corresponding output signal differences. The final relative uncertainty values are ranging from some tens of percent at the lower source temperatures (Sn and Zn), where the effect on the signal change is very small, about few percent at the higher source temperatures (Ag and Cu) where the effect on the output signal change is greater and it allows less uncertainty in the measurement. Experimental measurements have been performed at the fixed-points temperatures of: Sn, Zn, Ag and Cu. The temperature coefficient at the aluminium fixed-point was derived based on the trend observed at these other fixed points. No measurement and/or correction for internal temperature has been applied at the indium fixed point. The detailed measurement results and associated uncertainties are shown in Table 8.	The uncertainty budget for this component was derived by propagating the relative standard deviation of the difference in the measured internal temperature of the thermometer and the relative standard deviation of the corresponding output signal difference experimentally measured at the zinc point only. This standard relative uncertainty value (1.2 %) was therefore assumed representative also for calculating the internal temperature effect at the other fixed-points temperatures, simply by taking into account the sensitivity of the thermometer. The detailed measurement results and associated uncertainties are shown in Table 9.

u_i	**INRiM**	**UME**
Atmospheric absorption $u_{15}(T_i)$	The transfer standard radiation thermometer uses an interference filter with a peak wavelength centred at 1.6 µm and a working wavelength bandwidth (FWHM) of about 85 nm. Consequently, the full transmission curve of the interference filter lies in an atmospheric window "virtually" free from any atmospheric effects. Moreover, considering the short working distance (less than 1 m), the atmospheric absorption and emission effects might be considered negligible. However, to be conservative, an estimated residual atmospheric absorption effect with a relative uncertainty value of 0.01 %, corresponding to the "best" case shown in [9], was considered. On the base of this value and of the sensitivity of the thermometer, the corresponding relative uncertainty values in terms of temperature have been calculated at all fixed-points.	In all measurements, the radiation thermometer was employed at the same working distance equal to 470 mm. The measurements were done in a temperature and humidity-controlled environment. Considering the relatively short optical path, nearly constant (during the measurements) humidity values, and the relatively short working wavelength (about 1.6 µm) of the radiation thermometer, the uncertainty due to the atmospheric absorption and emission, according to the results of [2, 5], can be estimated to be negligible.

u_i	**INRiM**	**UME**
Gain ratios $u_{16}(T_i)$	Gain ratios measurements were performed using a Hewlett Packard Model 3458A calibrated digital multimeter. From its calibration certificate, the following relative standard uncertainties can be assumed as representative of the three different full scales used: - $3.5 \cdot 10^{-4}$ for background signals measurement of about 1 mV on the 100 mV full scale - $1.0 \cdot 10^{-6}$ for output signals of about 1 V on the 1 V full scale $8.5 \cdot 10^{-7}$ for output signals of about 10 V on the 10 V full scale The above standard uncertainty values, when propagated based on the equation used to determine the gain ratios values, give a final relative standard uncertainty due to multimeter calibration of approximately 0.00013 %. This value is more than two orders of magnitude lower when compared with the repeatability of the measurement of the gain ratios, so it can be completely neglected in the final uncertainty budget. Therefore, only the propagation of the contributions deriving from the repeatability of the sequence of successive measurements has been considered. A final standard uncertainty value of the order of magnitude of about 0.02 % was obtained. The detailed measurement results and associated uncertainties are shown in Table 5.	The gain ratio measurements were made by using the FP signals during the freezing plateau. The signal corresponding to each fixed point has been measured at the two adjacent gains together with the corresponding background signals. At least three sets of measurements were done for all gain ratios, (except the gain ratio $10^8/10^7$), and the corresponding average and standard deviations were calculated. In [12], this (method for the determination of the gain ratio using signals during the freezing plateau) was compared with the direct calibration of the amplifier using a current of a desired value (with sufficient accuracy) supplied to the input of the amplifier via a connected in series calibrated standard resistor R_{st}. For each gain setting, a standard resistor R_{st} with a nominal value that matches with the value of the corresponding feedback resistor of the amplifiers was used. At each gain setting, the gain factor $G(\mathrm{V \cdot A^{-1}})$ is calculated from the equation: $G = \frac{V_{amp}}{(V_{cal}/R_{st})}$, where V_{amp} is the amplifier output voltage, and *Vcal* is the output voltage of the DC voltage source. A good consistency of both methods in terms of absolute ratio value and measurement uncertainty was observed at all gain ratios, except the gain ratio $10^9/10^8$. At this gain ratio measurement, the uncertainty was relatively higher than at other gain ratios. This evaluation was assessed using In fixed-point freezing signal, where the detection of radiant energy is performed at the low limit of directivity of the InGaAs detector. The detailed measurement results and associated uncertainties are shown in Table 6.
	<u>Note:</u> *uncertainty in gain ratios measurements should only be considered when the thermometer calibration is compared over its entire working temperature range and not when only the respective signals at the fixed points have been compared (because, in this latter case, the same amplifier gains were used). Furthermore, in the former case, there is further convenience if the measured signals are normalized against the lower gain (used at the higher fixed-point temperature) because this produces a reduction in the calibration uncertainty due to the gain ratios measurements.*	

u_i	**INRiM**	**UME**
Noise $u_{17}(T_i)$	The performance of the thermometer's transimpedance amplifier at each gain setting is such that its noise is less than that resulting from the temperature stability of any source being measured. With this hypothesis, based on experimental evidences, the standard deviation of the measured background signal can be assumed as the final limit for the noise parameter. It is possible to determine the corresponding noise equivalent temperature difference (NETD) as a function of the temperature of the source, knowing the gain used and the calculated sensitivity of the thermometer. The resolution of the thermometer's temperature reading ranges from 3.2 mK at the indium point and improves to a few hundredths of a millikelvin at the highest source temperatures.	In the measurements, a Digital Multimeter HP3458 Option A was used. According to its calibration certificate at the moment of the comparison measurements, it had the following relative standard uncertainties: • $1.5 \cdot 10^{-4}$ for output signals measurement of about 10 mV on the 100 mV full scale; • $0.7 \cdot 10^{-6}$ for output signals of about 1 V on the 1 V full scale; • $2.0 \cdot 10^{-7}$ for output signals of about 10 V on the 10 V full scale. These values obtained from the calibration certificate of the HP3458A, together with the calculated sensitivities at each fixed point, were used to determine the noise (i.e., the uncertainty due to voltmeter quantisation) expressed in terms of temperature.
Interpolation error $u_{18}(T_i)$	The uncertainty due to interpolation error can be calculated on the base of the equations described and recommended in [9] and reported as in following: $u_{18} = \frac{\lvert E \rvert \lambda_0^2 T_{range}^3}{36}$ Where: λ_0 is the nominal working wavelength of the thermometer (1.6 µm in our case), T_{range} is the corresponding calibration temperature range (i.e., $T_{Cu} - T_{In}$), and E is given by: $\lvert E \rvert = \frac{c_2^2}{12x^4}\left[1 - \frac{1}{[1-\exp(-c_2/x)]^2}\right]$ where: $x = \lambda_0 \cdot T_m$ and T_m is the mean of the temperatures used to determine the parameters of the interpolation equation. Considering that for radiation thermometers with working wavelengths of 1.6 µm, both the Planck and Wien versions of the Sakuma–Hattori equation give results of the same orders of magnitude, a final uncertainty value for the interpolation error of about 20 mK may be accounted for.	
	<u>Note:</u> *as for the gain ratios, also in this case, this uncertainty component must be taken into account only when comparing the calibration of the thermometer over its entire working temperature range and not when comparing only the respective signals at the fixed points.*	
Drift $u_{19}(T_i)$	During the characterization and calibration process of the thermometer, the reference zinc fixed point was used to check for any drifts. The signals measured at the other fixed points were then corrected using the corresponding calculated relative change. The uncertainty component due to the stability of the instrument (drift) has been derived by taking into account all the measurements done using the Zn fixed-point reference at both Institutes during all the comparison time. The uncertainty component due to the drift has been estimated to be 38 mK at the freezing point of zinc. This value was derived from the median standard error of all Zn checks performed. The effect of this uncertainty component was then propagated at the temperatures of the other fixed points on the base of the sensitivity of the thermometer using as the sensitivity coefficient the expression $(T/T_{ref})^2$. This method produced the following results in terms of uncertainty: 15 mK at the indium point, 20 mK at the tin, 70 mK at the aluminium, 122 mK at the silver and 148 mK at the copper fixed point, respectively.	

Table 15: Summary of the uncertainty components considered in the FPBB calibration scheme.

The estimated values for the uncertainty components, together with total combined uncertainty and expanded uncertainty, are reported in Tables 16 and 17 for INRiM and UME, respectively.

	Quantity	/						
		xls abs time	43395	43376	43397	43409	43403	43411
Fixed Points Calibration	Date of meas.	dd/mm/yyyy	22/10/2018	03/10/2018	24/10/2018	05/11/2018	30/10/2018	07/11/2018
INRiM	Fixed Point		In	Sn	Zn	Al	Ag	Cu
	FP temperature	°C	156.5985	231.928	419.527	660.323	961.78	1084.62
	TS1 Sensitivity	%/°C	4.8691338	3.5250359	1.8742129	1.0319934	0.5896520	0.4877845
	Gain used 10^X	V/A	9	9	7	6	5	5
Description								
Impurities	$u_2(T_i)$	mK	2.7	1.7	3.5	3.9	6.5	10
Plateau identification	$u_3(T_i)$	mK	10	2.0	2.0	2.0	3.9	11
Blackbody emissivity, isothermal (relative unc.)	$u_4(S_i)/S_i$	%	0.010	0.010	0.010	0.010	0.010	0.010
Blackbody emissivity, isothermal	$u_4(T_i)$	mK	2.1	2.8	5.3	9.7	17	21
Reflected ambient radiation	$u_6(T_i)$	mK	0	0	0	0	0	0
Cavity bottom heat exchange	$u_7(T_i)$	mK	0.1	0.2	0.9	3.0	9.4	14
Size-of-source-effect correction (relative unc.) (*)	$u_{11}(S_i)/S_i$	%	5.1	5.3	5.2	17	19	16
Size-of-source-effect correction	$u_{11}(T_i)$	mK	0.3	0.5	0.8	1.8	3.2	3.9
Non-linearity (relative unc.)	$u_{12}(S_i)/S_i$	%	5.0E-03	5.0E-03	5.0E-03	5.0E-03	5.0E-03	5.0E-03
Non-linearity	$u_{12}(T_i)$	mK	1.0	1.4	2.7	4.8	8.5	10
Ambient temperature correction (relative unc.)	$u_{14}(S_i)/S_i$	%	0	36	7.3	7.0	6.4	2.6
Ambient temperature correction	$u_{14}(T_i)$	mK	0.0	0.2	0.2	0.2	6.0	4.5
Atmospheric absorption (relative unc.)	$u_{15}(S_i)/S_i$	%	0.01	0.01	0.01	0.01	0.01	0.01
Atmospheric absorption	$u_{15}(T_i)$	mK	2.1	2.8	5.3	9.7	17	21
Gain ratios (relative unc.)	$u_{16}(S_i)/S_i$	%	0.0	0.0	0.0	0.0	0.0	0.0
Gain ratios	$u_{16}(T_i)$	mK	0.0	0.0	0.0	0.0	0.0	0.0
Noise	$u_{17}(T_i)$	mK	3.2	0.84	0.021	0.013	0.017	0.015
Interpolation error	$u_{18}(T_i)$	mK	0.0	0.0	0.0	0.0	0.0	0.0
Drift	$u_{19}(T_i)$	mK	15	20	38	70	122	148
Total Combined Uncertainty	u_c	mK	19	21	39	72	125	153
Coverage Factor	k = 2							
Expanded Uncertainty	$U_{k=2}$	mK	**38**	**41**	**78**	**143**	**251**	**305**

(*) relative uncertainty expressed on the SSE correction

Table 16: Fixed-points blackbody calibration scheme – INRiM uncertainties.

	Quantity	/						
		xls abs time	44093	44096	44085	44087	44088	44100
Fixed Points Calibration	Date of meas.	dd/mm/yyyy	19/09/2020	22/09/2020	11/09/2020	13/09/2020	14/09/2020	26/09/2020
UME	Fixed Point		In	Sn	Zn	Al	Ag	Cu
	FP temperature	°C	156.5985	231.928	419.527	660.323	961.78	1084.62
	TS1 Sensitivity	%/°C	4.8691338	3.5250359	1.8742129	1.0319934	0.5896520	0.4877845
	Gain used 10^X	V/A	9	9	7	6	5	5
Description								
Impurities	$u_2(T_i)$	mK	5.0	5.0	5.0	7	11	12
Plateau identification	$u_3(T_i)$	mK	13	10	8.0	6.0	12	18
Blackbody emissivity, isothermal (relative unc.)	$u_4(S_i)/S_i$	%	0.001	0.002	0.001	0.001	0.001	0.001
Blackbody emissivity, isothermal	$u_4(T_i)$	mK	0.3	0.4	0.8	1.3	2.5	2.7
Reflected ambient radiation	$u_6(T_i)$	mK	0	0	0	0	0	0
Cavity bottom heat exchange	$u_7(T_i)$	mK	5.0	5.0	5.0	5.0	25	35
Size-of-source-effect correction (relative unc.) (**)	$u_{11}(S_i)/S_i$	%	1.84E-02	1.84E-02	1.84E-02	1.84E-02	1.84E-02	1.84E-02
Size-of-source-effect correction	$u_{11}(T_i)$	mK	3.8	5.2	9.8	18	31	38
Non-linearity (relative unc.)	$u_{12}(S_i)/S_i$	%	0.0E+00	0.0E+00	0.0E+00	0.0E+00	0.0E+00	0.0E+00
Non-linearity	$u_{12}(T_i)$	mK	0.0	0.0	0.0	0.0	0.0	0
Ambient temperature correction (relative unc.)	$u_{14}(S_i)/S_i$	%	1.7	1.7	1.2	1.7	1.7	1.7
Ambient temperature correction	$u_{14}(T_i)$	mK	0.3	0.3	0.4	0.0	0.2	0.6
Atmospheric absorption (relative unc.)	$u_{15}(S_i)/S_i$	%	0	0	0	0	0	0
Atmospheric absorption	$u_{15}(T_i)$	mK	0.0	0.0	0.0	0.0	0	0
Gain ratios (relative unc.)	$u_{16}(S_i)/S_i$	%	0.0	0.0	0.0	0.0	0.0	0.0
Gain ratios	$u_{16}(T_i)$	mK	0.0	0.0	0.0	0.0	0.0	0.0
Noise	$u_{17}(T_i)$	mK	3.99	0.14	0.02	0.03	0.29	0.05
Interpolation error	$u_{18}(T_i)$	mK	0.0	0.0	0.0	0.0	0.0	0.0
Drift	$u_{19}(T_i)$	mK	15.0	20.0	38.0	70.0	122	148
Total Combined Uncertainty	u_c	mK	22	24	41	73	129	158
Coverage Factor	k = 2							
Expanded Uncertainty	$U_{k=2}$	mK	**44**	**48**	**81**	**146**	**259**	**316**

(**) relative uncertainty expressed on the full signal

Table 17: Fixed-points blackbody calibration scheme – UME uncertainties.

8 FIXED-POINTS CALIBRATION: ANALYSIS OF RESULTS, DISCUSSION AND CONCLUSIONS

The transfer standard radiation thermometer INRiM TS1 has been calibrated, by both Institutes, in the temperature range between 156.5985 °C and 1084.62 °C following the fixed-points blackbody technique. The measurement results at the fixed-points and the associated uncertainties are summarised in Tables 12, 14, 16 and 17 for INRiM and UME, respectively. The protocol recommended calculating the comparison reference value (CRV) at each fixed point using the weighted mean of the individual results of the participants. The standard uncertainty associated with the CRV will be then given by the root mean square sum of the respective standard measurement uncertainties. By performing the above process, the following comparison reference values and expanded uncertainties were derived at the different fixed points:

	In	Sn	Zn	Al	Ag	Cu	
CRV	*83.25*	*1827.9*	*1977.2*	*5469.9*	*5641.6*	*10863*	(mV)
$U_{k=2}$	*0.17*	*2.9*	*3.0*	*8.2*	*8.5*	*16*	(mV)
$U_{k=2}$	**41**	**45**	**80**	**145**	**255**	**311**	(mK)

Table 18: Comparison reference values (CRV) and standard uncertainties.

Signals and temperature differences with respect to the CRV were then calculated for INRiM and UME, respectively. The values found are numerically reported in Table 19 and graphically shown in Figure 20, together with expanded uncertainty bars ($U_{k=2}$) and CRV uncertainty limits.

	In	Sn	Zn	Al	Ag	Cu	
INRiM - CRV	*0.238*	*1.85*	*0.54*	*4.37*	*-0.36*	*-1.24*	(mV)
	58.5	28.6	14.6	77.4	-10.8	-23.3	(mK)
$U_{k=2}$	**38**	**41**	**78**	**143**	**251**	**305**	(mK)
UME - CRV	*-0.315*	*-2.49*	*-0.59*	*-4.51*	*0.38*	*1.33*	(mV)
	-77.9	-38.7	-15.8	-80.0	11.5	25.1	(mK)
$U_{k=2}$	**44**	**48**	**81**	**146**	**259**	**316**	(mK)

Table 19: Signals and temperature differences with respect to the CRV values.

The results shown in Figure 20 highlight two different aspects that seem to be clearly at odds with each other. In particular, a much better agreement was found at higher temperatures (i.e. at the silver and copper fixed points) than at the other fixed points (i.e., at and below the aluminium fixed point).

However, by considering and analysing all the uncertainty components estimated by each NMIs becomes clear that the greater effect on the overall uncertainty in the comparison exercise arises from the stability of the transfer standard thermometer over the time.

This uncertainty value, due to a possible drift of the thermometer, was accounted for and propagated at the temperatures of the other fixed points based on the drift observed at the zinc reference point, which accompanied the thermometer throughout the comparison period. While this assumption may be correct in principle, it is made and based on the assumption that only the sensitivity of the detector has changed and that the same transimpedance amplifier gain is used at all fixed points, but this is not the case.

From the results obtained, there seems to be clear evidence of an overestimation of the uncertainty of the drift effect in the higher temperature range (where lower amplifier gains have been used and consequently smaller valued and more stable feedback resistors) than those at the lower temperatures, where the reverse occurs.

From and below the aluminium fixed-point temperature, increased temperature differences with respect to the CRV were observed for both NMI measurements. However, excluding only the fixed point of indium, where strictly speaking the measurements of both NMI can be considered just barely compatible with the CRV, at all other fixed points temperatures, a good overlapping of the respective uncertainty bars can be observed, which gives an indication of the agreement between the measurement results.

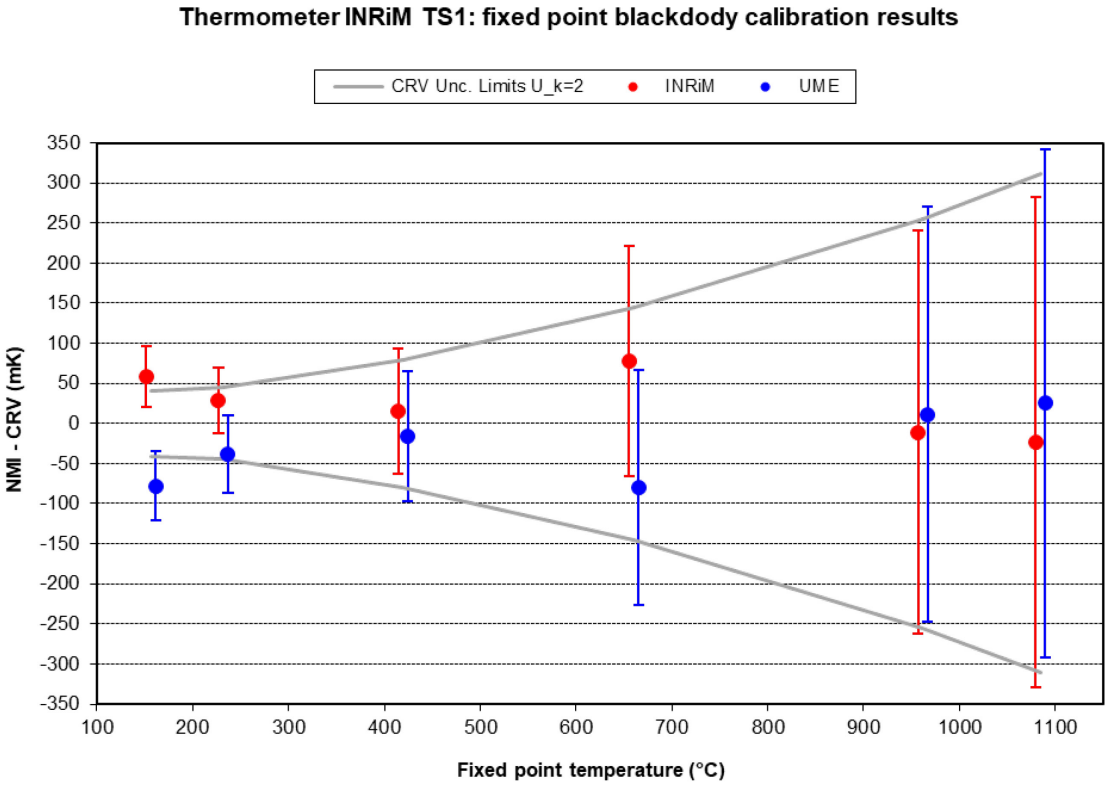

Note: *the values of the fixed-points' temperature on the X-axis of the graph have been slightly shifted with respect to their nominal values only to avoid the overlapping of the uncertainty bars*

Figure 20: Fixed points calibration temperature differences with respect to the CRV.

Interesting and direct outcomes of the present comparison exercise may be:

1) the need for a different way to evaluate the propagation of uncertainty due to the stability of the thermometer at temperatures other than the one taken as a reference (i.e. the zinc fixed point) which takes into account the different range of gains used by the transimpedance amplifier;

2) a comparison of the calibration results over the entire working temperature range of the thermometer (and not only at the fixed-points temperatures). So that the measurements of the gain ratios, the process of normalization of the signals, the interpolation equation used and the possible non-linearity can play an important key role in determining the true final uncertainty value.

REFERENCES

[1] F. Girard, "*Studio, realizzazione e caratterizzazione di un termometro ad infrarosso campione di trasferimento nel campo di temperatura tra 150 °C e 1000 °C*", Università degli Studi di Torino, Facoltà di Scienze M.F.N., Corso di Laurea in Fisica, Tesi di Laurea, A.A. 1998-1999

[2] M. Battuello, F. Girard, T. Ricolfi, "*An improved version of the IMGC InGaAs precision infrared thermometer*", Proceedings of the 9th International Symposium on temperature and Thermal Measurements in Industry and Science (TEMPMEKO 2004) pp. 505-508

[3] F. Girard, T. Ricolfi, "*A transportable blackbody furnace for the accurate realization of the fixed points of indium, tin and zinc*", Meas. Sci. Technol. 9, 1215-1218 (1998)

https://dx.doi.org/10.1088/0957-0233/9/8/012

[4] M. Battuello, F. Lanza, T. Ricolfi: "*Fixed-Point Technique for Approximating the ITS-90 between 420 °C and 1085 °C with an Infrared Thermometer*", Metrologia 27, 75-82 (1990)

http://dx.doi.org/10.1088/0026-1394/27/2/005

[5] E.W.M. van der Ham, M. Battuello, P. Bloembergen, R. Bosma, S. Clausen, O. Enouf, E. Filipe, J. Fischer, B. Gutschwager, T. Hirvonen, J.U. Holtoug, J. Ivarson, G. Machin, H. McEvoy, J. Peres, T. Ricolfi, P. Ridoux, M. Sadli, V. Schmidt, C. Staniewicz, O. Struss, T. Weckstrom, F. Girard, "*TRIRAT: Traceability in infrared radiation thermometry from −50 °C to 800 °C*", Framework 4 Project of the Standards, Measurement and Testing Programme of the European Commission, Contract No. SMT 4-CT-96-2060

[6] H. McEvoy, M. J. Martin, A. Steiner, E. Schreiber, F. Girard, M. Battuello, M. Sadli, P. Ridoux, B. Gutschwager, J. Hollandt, A. Diril, Ö. Pehlivan, "*Report on the measurement results for the EURAMET 658 extension: project to examine underlying parameters in radiance scale realization*", Metrologia, 2018, 55 (1A), 03001

http://dx.doi.org/10.1088/0026-1394/55/1A/03001

[7] G. Machin and M. Ibrahim "*SSE and temperature uncertainty: I-High temperature systems*", in Proceedings of TEMPMEKO 99, pp. 681-686

[8] P. Bloembergen and Y. Yamada "*The impact of the SSE on the uncertainty of fixed-point radiance temperatures: a case study*", in Proceedings of TEMPMEKO 2004, pp. 1141-1148.

[9] P. Saunders, J. Fischer, M. Sadli, et al. Int. J Thermophys (2008) 29: 1066.

https://doi.org/10.1007/s10765-008-0385-1

[10] H. W. Yoon, J. J. Butler, T. C. Larason, G. P. Eppeldauer, "*Linearity of InGaAs photodiodes*", Metrologia, 40, S154–S158, 2003.

https://doi.org/10.1088/0026-1394/40/1/335

[11] M. Battuello, P. Bloembergen, F. Girard, T. Ricolfi, "*A comparison of two methods for measuring the nonlinearity of infrared radiation thermometers*", in Temperature: Its Measurement and Control in Science and Industry, Vol. 7, edited by D C Ripple et al., AIP Conference Proceedings, Melville, New York, 613–618, 2003.

[12] H. Nasibov, A. Diril, O. Pehlivan and M. Kalemci, "*Comparative study of two InGaAs-based reference radiation thermometers*", Int. J. Thermophys (2017), 38: 1–13

https://doi.org/10.1007/s10765-017-2245-3